國立彰化師範大學電子工程學系研究所研討會

變晶式高電子移動率電晶體

Metamorphic High Electron Mobility Transistors (MHEMTs)

主講人： 李 景 松 副教授
逢甲大學電子工程學系

Dec. 30, 2005

Outline

I. Introduction:

- Why needs “high-frequency” devices ?
- Why uses “compound” semiconductors ?
- How to enable “high electron-mobility” ?
- Why needs “metamorphic” devices ?

II. Some Device Designs:

- δ-Doped InAlAs/InGaAs/GaAs MHEMTs with Different Channel Structures
- Parameter Extraction for RF Model Build-Up
- Gate-Alloy-Related Kink Effects for MHEMTs

III. Conclusions

Q&A

I. Introduction

- **Why needs “high-frequency” devices ?**

To provide component recipes for monolithic microwave/millimeter-wave integrated circuit (MMIC) applications.

Microwave: 0.1 GHz ~ 30 GHz
Millimeter wave: 30 GHz ~ 300 GHz

- **Why using “compound” semiconductors ?**

1. Intrinsic high-speed property:

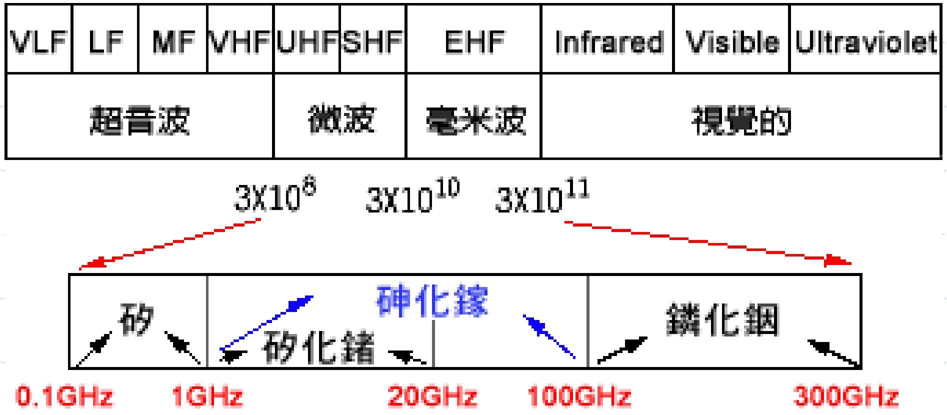

I. Introduction

- **Why using “compound” semiconductors ? (continued)**

2. Optical coupling capability:
   Suitable for opto-electronic integrated circuit (OEIC) implementations.
3. Controllable and composition-dependent material properties:
4. Variety of compound materials:
   Both provide high degree of design freedom.
5. Mature epitaxy growth technologies:
   LP-MOCVD, MBE…
   Make possible excellent precision control of layer thickness and cost-effective mass-production.

I. Introduction

How to enable "high electron-mobility" ?

- By spatially separating electrons from their parent donors to greatly improve the ionized-impurity scattering .
- By devising an undoped channel compound, with high saturation velocity, where the transferred two-dimensional electron gas (2DEG) are confined and transport along under applied bias.

→ High Speed !!

Schematic band diagram of a conventional HEMT:

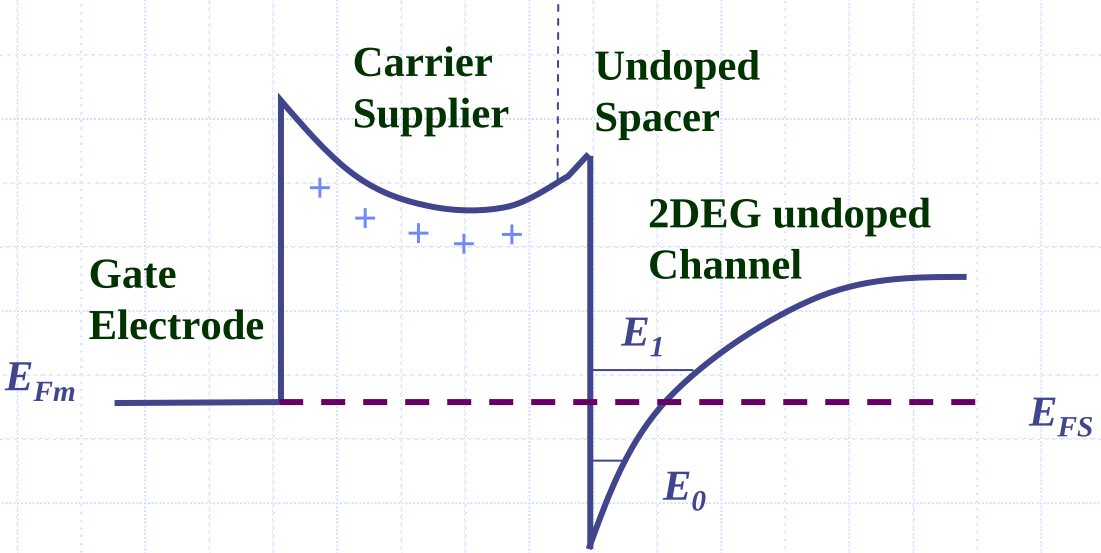

I. Introduction

Why needs "metamorphic" devices ?

-- Comparisons between InP-based and GaAs-based HEMTs:

- Advantages of InP-based HEMTs:
  - Lattice-matched to higher In-composition InGaAs compounds.
  - Lower effective electron mass.
  - Higher electron mobility and saturation velocity.
  - Larger conduction band discontinuity (ΔE_C).
  - Higher two-dimensional electron gas (2-DEG) carrier density.

- Applications of InP-based HEMTs:
  - High drain current density.
  - High voltage and power gains.
  - High cutoff frequency.
  - Low noise.

I. Introduction

- Disadvantages of InP substrates as compared to GaAs substrates:
  - Mechanically fragile.
  - Limited wafer-size.
  - Expensive.

To integrate the high-speed compounds onto robust GaAs substrates with larger wafer-size

Metamorphic HEMTs (MHEMTs)

I. Introduction

Metamorphic Buffer:

- Two major functions of using metamorphic buffer :
  1) to accommodate the large lattice-mismatch between GaAs substrate and the active layers
  2) to prevent the dislocations from being injected into the device channel

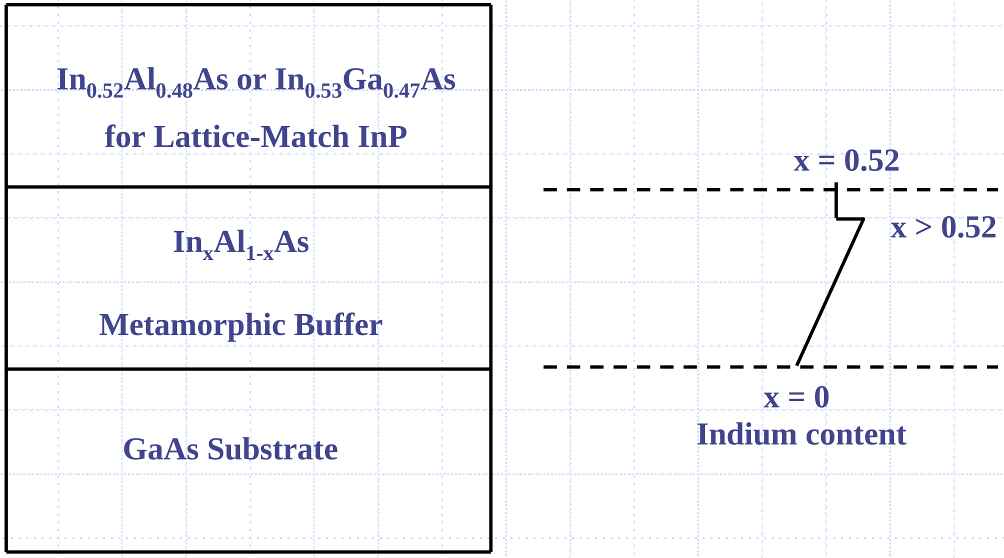
$In_{0.52}Al_{0.48}As$ or $In_{0.53}Ga_{0.47}As$ for Lattice-Match InP

$In_xAl_{1-x}As$ Metamorphic Buffer

GaAs Substrate

Inverse-step buffer:
to provide good relaxation
for the strained active layers

II. Some Device Designs

- **δ-Doped InAlAs/InGaAs/GaAs MHEMTs with Different Channel Structures:**

  - **PC-MHEMT:**

    δ-Doped $In_{0.425}Al_{0.575}As/In_{0.65}Ga_{0.35}As/GaAs$ Pseudomorphic Channel MHEMT

  - **SGC-MHEMT:**

    δ-Doped $In_{0.425}Al_{0.575}As/In_{x}Ga_{1-x}As$ ($x = 0.5 \rightarrow 0.65 \rightarrow 0.5$)/GaAs Symmetrically-Graded Channel MHEMT

II. Some Device Designs

- **Schematic cross section for the PC-MHEMT:**

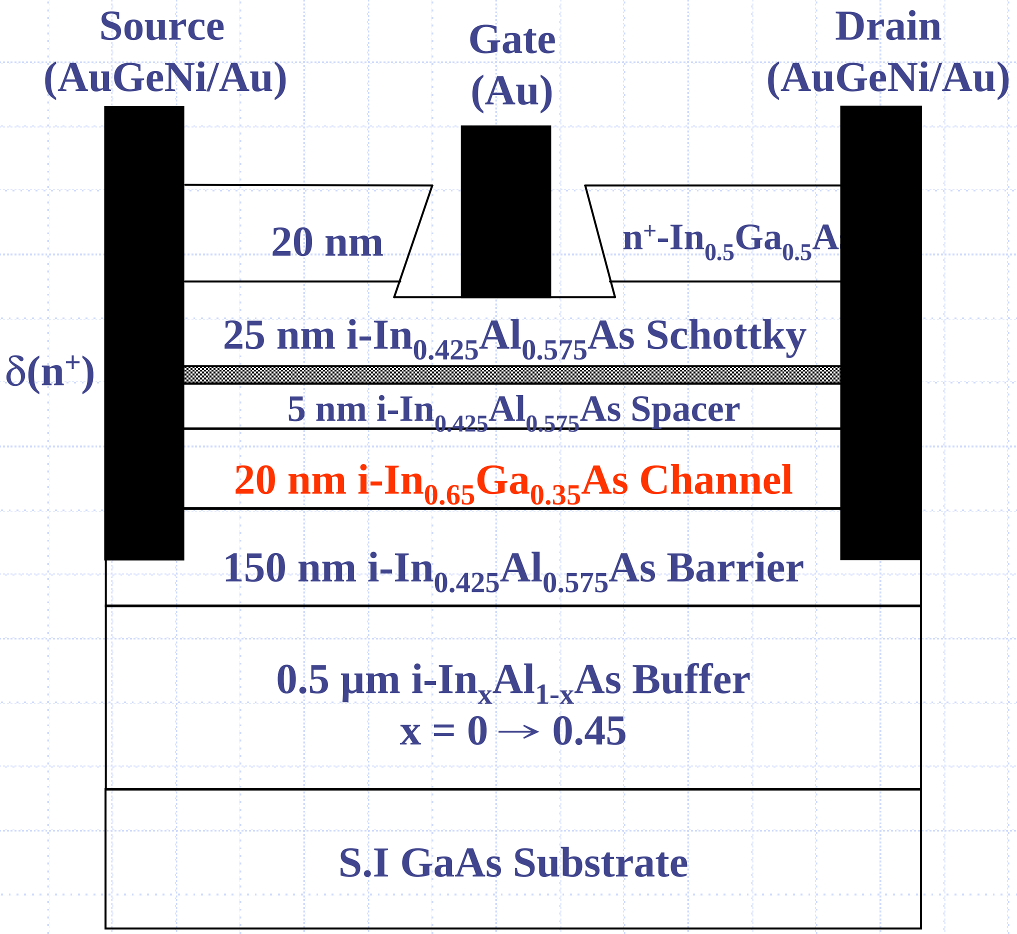

Source
(AuGeNi/Au)

Gate
(Au)

Drain
(AuGeNi/Au)

20 nm

n^{+}-In$_{0.5}$Ga$_{0.5}$A

25 nm i-In$_{0.425}$Al$_{0.575}$As Schottky

$\delta(n^{+})$

5 nm i-In$_{0.425}$Al$_{0.575}$As Spacer

20 nm i-In$_{0.65}$Ga$_{0.35}$As Channel

150 nm i-In$_{0.425}$Al$_{0.575}$As Barrier

0.5 μm i-In$_{x}$Al$_{1-x}$As Buffer
$x = 0 \rightarrow 0.45$

S.I GaAs Substrate

- **Gate dimension :**
  $0.65 \times 200\ \mu m^2$

II. Some Device Designs

- **Schematic cross section for the SGC-MHEMT:**

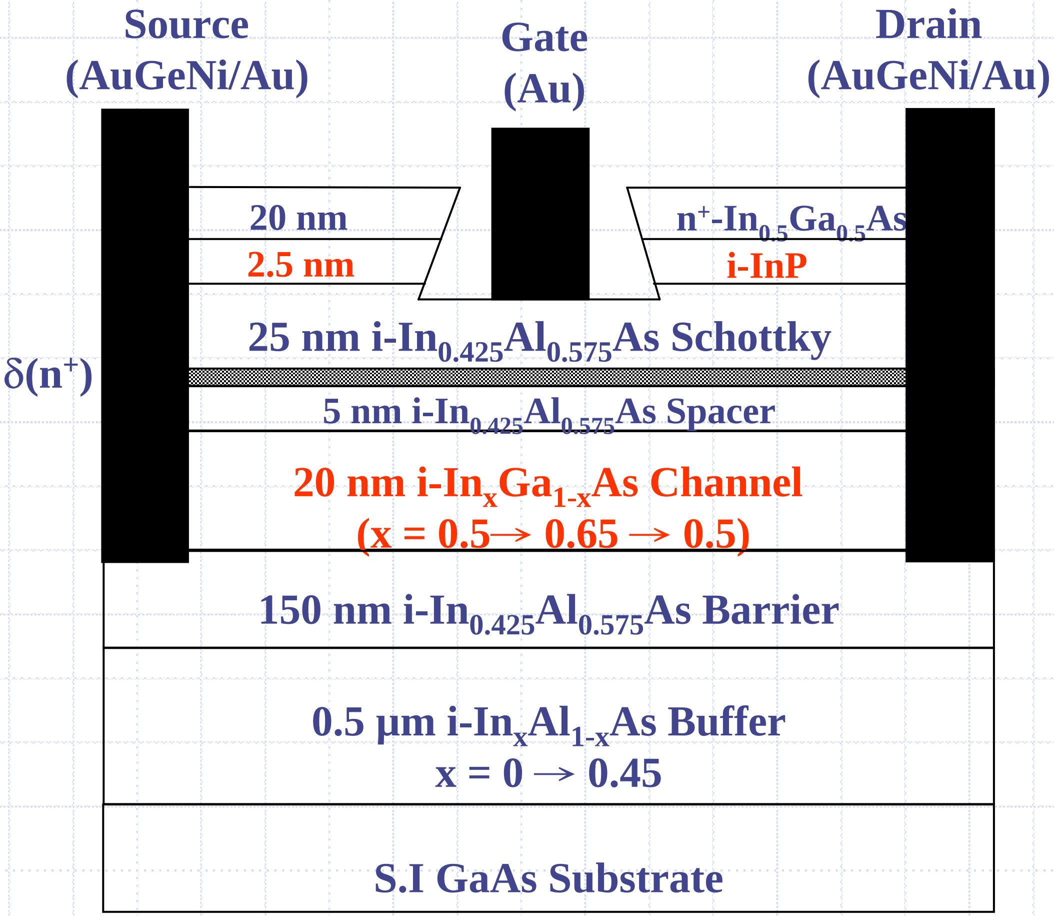

Source
(AuGeNi/Au)

Gate
(Au)

Drain
(AuGeNi/Au)

20 nm

2.5 nm

n^+-$In_{0.5}Ga_{0.5}As$

i-InP

25 nm i-$In_{0.425}Al_{0.575}As$ Schottky

$\delta(n^+)$

5 nm i-$In_{0.425}Al_{0.575}As$ Spacer

20 nm i-$In_xGa_{1-x}As$ Channel
($x = 0.5 \rightarrow 0.65 \rightarrow 0.5$)

150 nm i-$In_{0.425}Al_{0.575}As$ Barrier

0.5 μm i-$In_xAl_{1-x}As$ Buffer
$x = 0 \rightarrow 0.45$

S.I GaAs Substrate

- **Gate dimension** :
  $0.65 \times 200\ \mu m^2$

II. Some Device Designs

Mechanism of the kink effect:

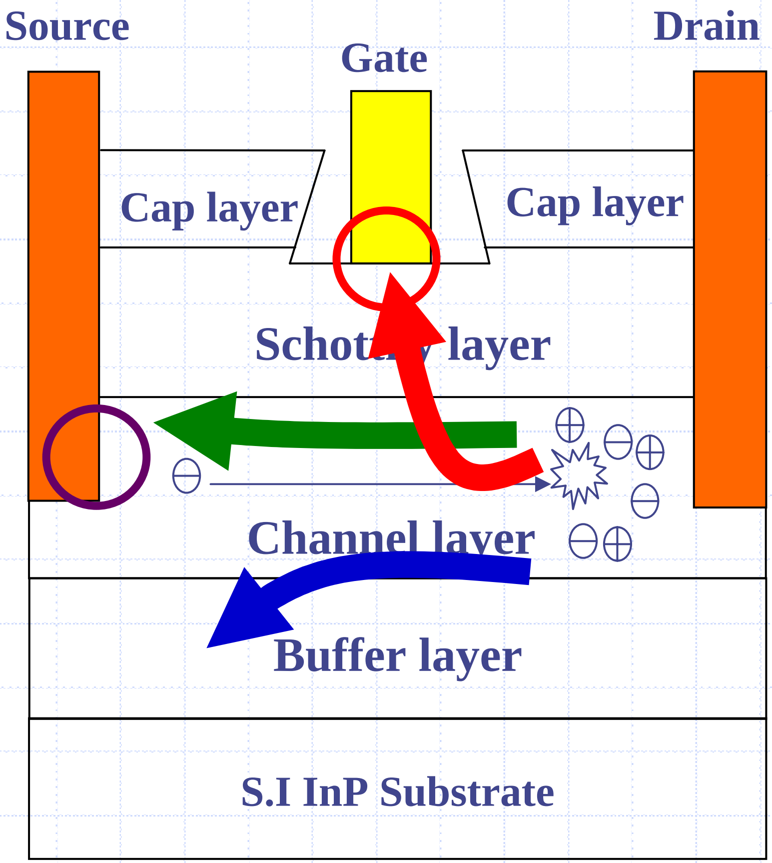

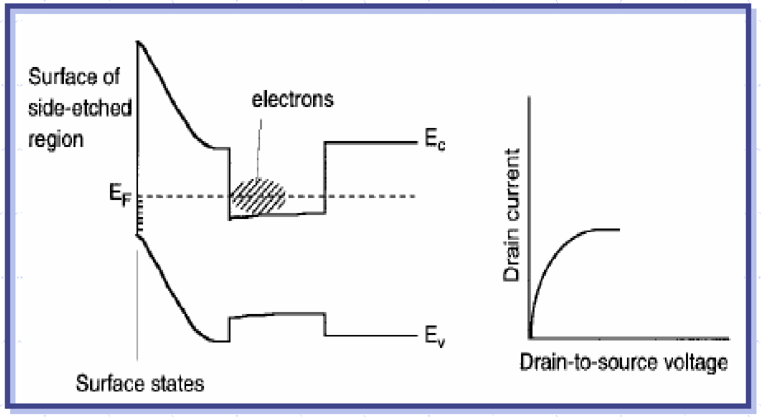

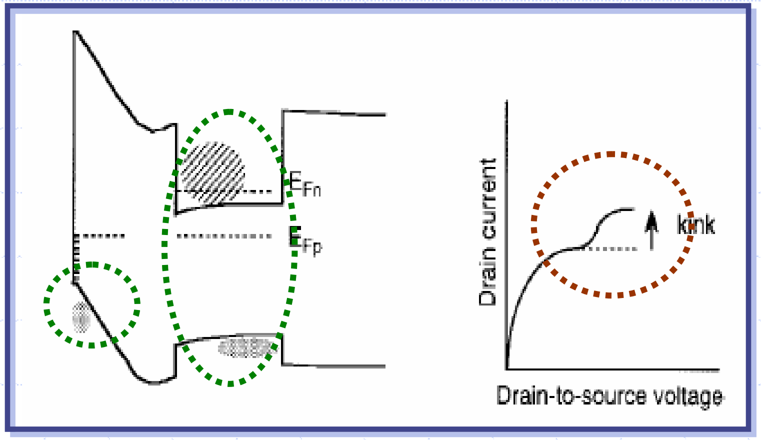

II. Some Device Designs

- Insertion of an InP layer on the InAlAs structure provides:
  (1) Selective etching between InP and InAlAs can improve the processing reproducibility and the threshold uniformity.
  (2) Suppression of kink effects by passivating the deep levels on the InAlAs interface.

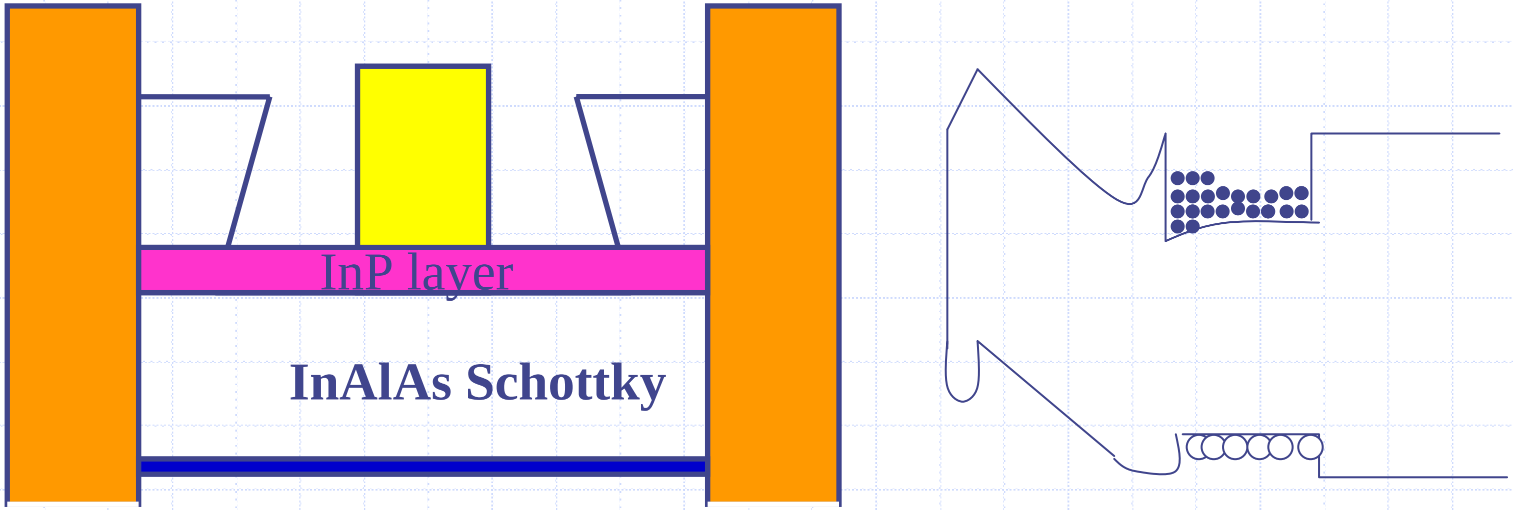

$g_m(f)$ Dispersion

- **Verified by the transconductance frequency dispersion measurement:**

without InP

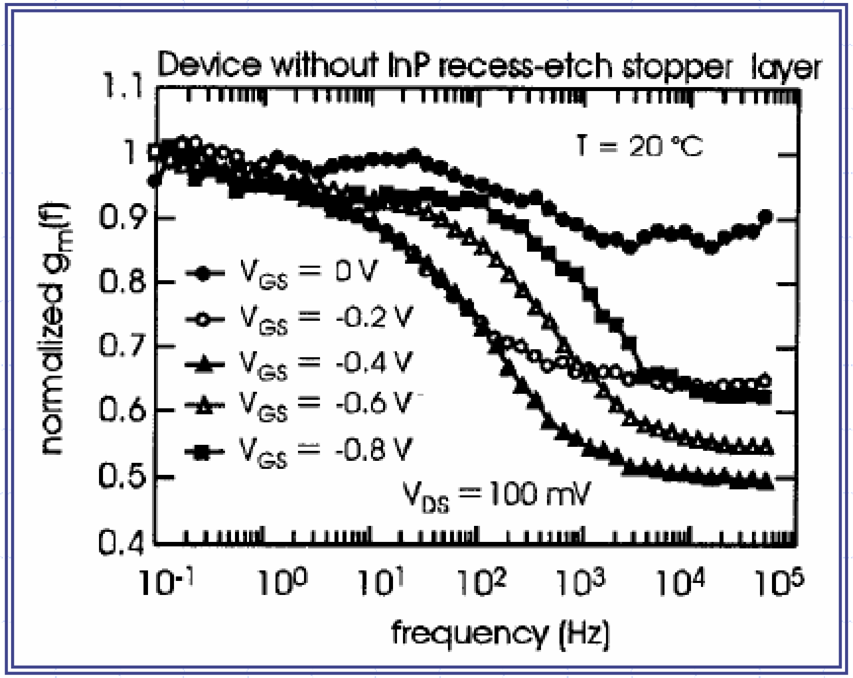

with InP

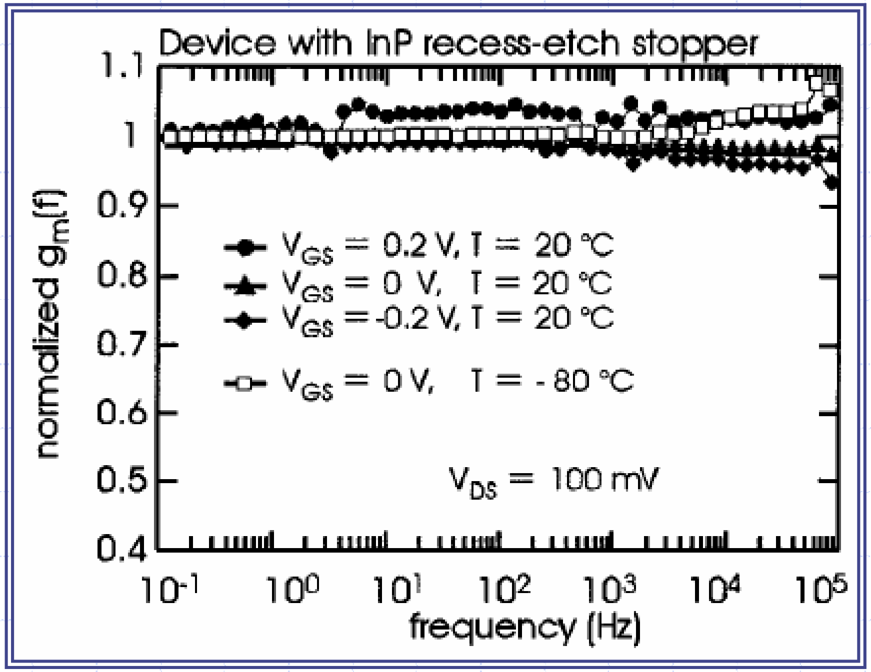

***Electron Devices Meeting, 1998. IEDM '98 Technical Digest., International 6-9 Dec. 1998 Page(s): 227 – 230.**

II. Some Device Designs

Expectations for PC-MHEMT and SGC-MHEMT :

- Advantages of PC-MHEMT ($In_{0.65}Ga_{0.35}As$) :
  - better carrier transport properties
  - larger conduction band discontinuities
  - improved carrier confinement capability
- Expected improved characteristics of PC-MHEMT include :
  - drain current and transconductance
  - high-frequency characteristics
  - noise performances
  - thermal stability

→ high-speed, low-noise and high-temperature applications

II. Some Device Designs

- Disadvantages of PC-MHEMT :
  - impact-ionization and kink effects
  - degraded output conductance
  - low breakdown voltages
  - narrow gate-voltage-swing (GVS)

- Advantages of SGC-MHEMT ($x = 0.5 \rightarrow 0.65 \rightarrow 0.5$) :
  - Larger effective energy band-gap:
    - to improve impact-ionization and kink effects
    - to decrease output conductance
    - to improve breakdown voltages

high power applications

  - Uniform distribution of carriers in channel:
    - to achieve a wider gate-voltage swing

high linearity applications

II. Some Device Designs

- **Schematic band diagrams for PC-MHEMT and SGC-MHEMT:**

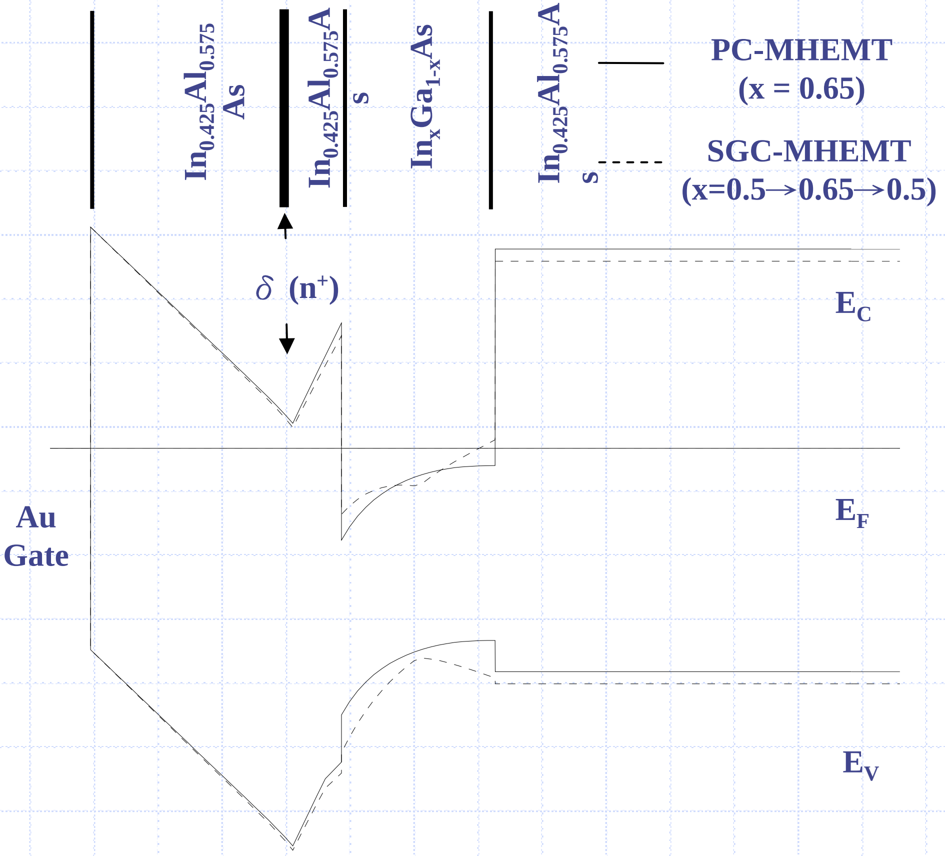

II. Some Device Designs

- **Comparisons of Hall measurement results between PC-MHEMT and SGC-MHEMT:**

Hall Characteristics	PC-MHEMT (x = 0.65)	SGC-MHEMT (x = 0.5→0.65→0.5)
Electron Mobility (cm^2/V-s) at 300 K (77 K)	7209 (32937)	7059 (30559)
2DEG Concentrations (× 10^{12} cm^{-2}) at 300 K (77 K)	4.1 (3.6)	3.8 (3.7)
Mobility-Concentration Product (× 10^{16} 1/V-s) at 300 K (77 K)	2.96 (11.8)	2.68 (11.3)

II. Some Device Designs

- **I-V characteristics of PC-MHEMT and SGC-MHEMT:**

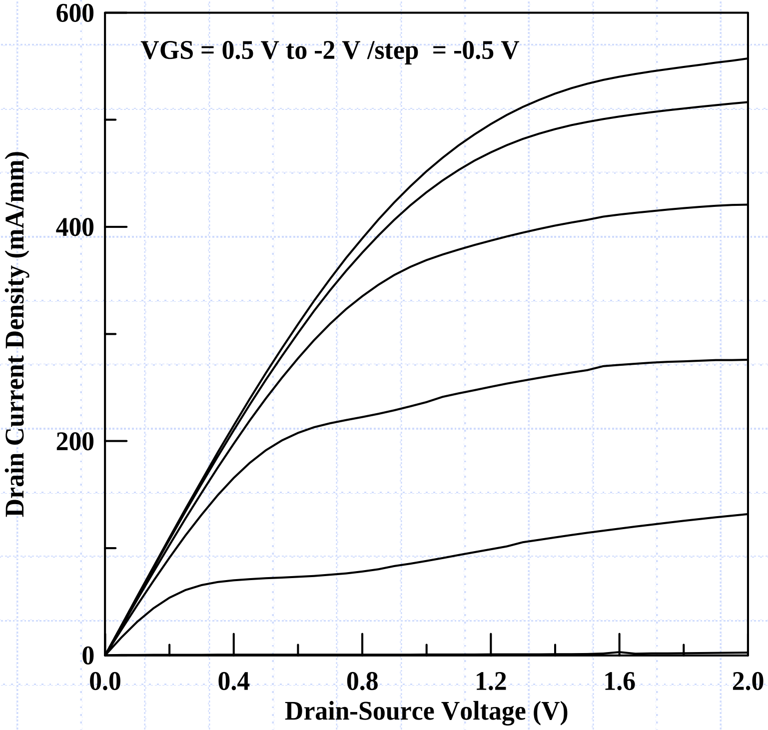

PC-MHEMT

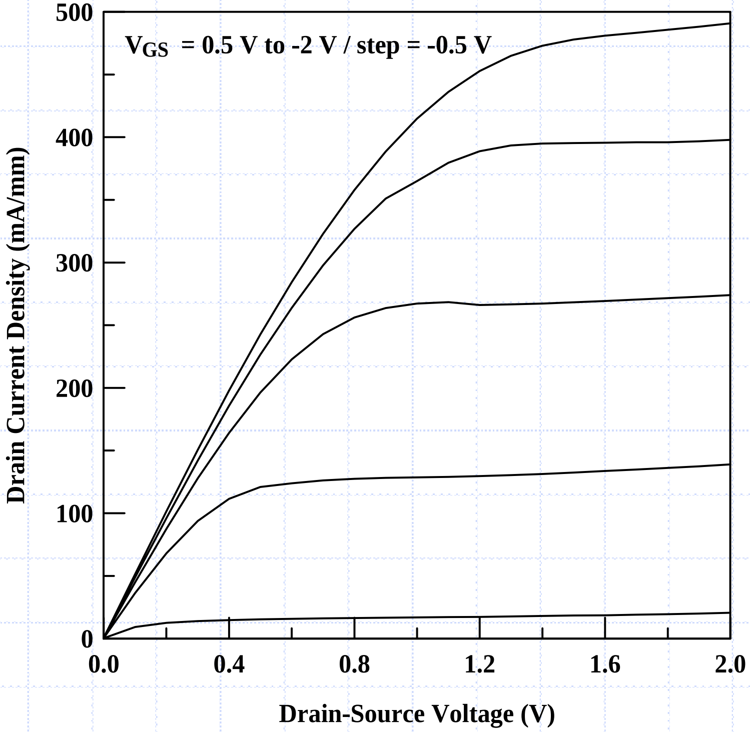

SGC-MHEMT

II. Some Device Designs

- g_m and g_d characteristics as a function of V_{DS} :

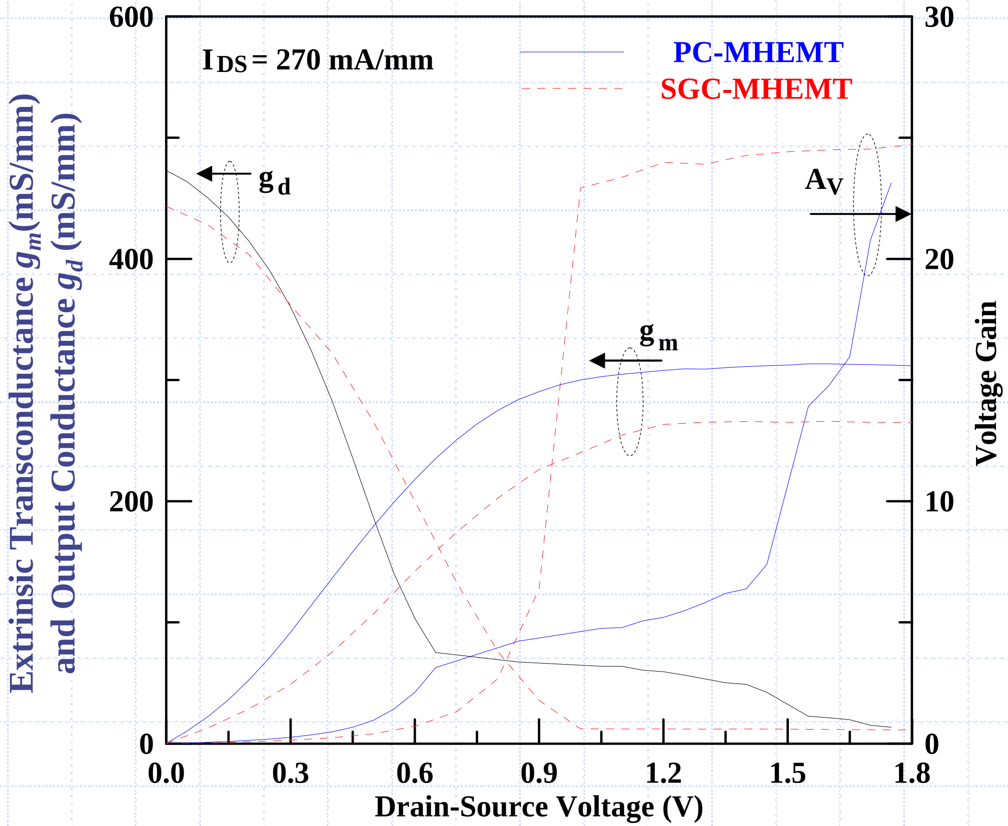

- **For PC-MHEMT**
  - g_d = 13.5 mS/mm
  - Av = 23.2 V
- **For SGC-MHEMT**
  - g_d = 11 mS/mm
  - Av = 24.6 V

at V_{DS} = 1.75 V

II. Some Device Designs

I_{DSS} and g_m vs. V_{GS} :

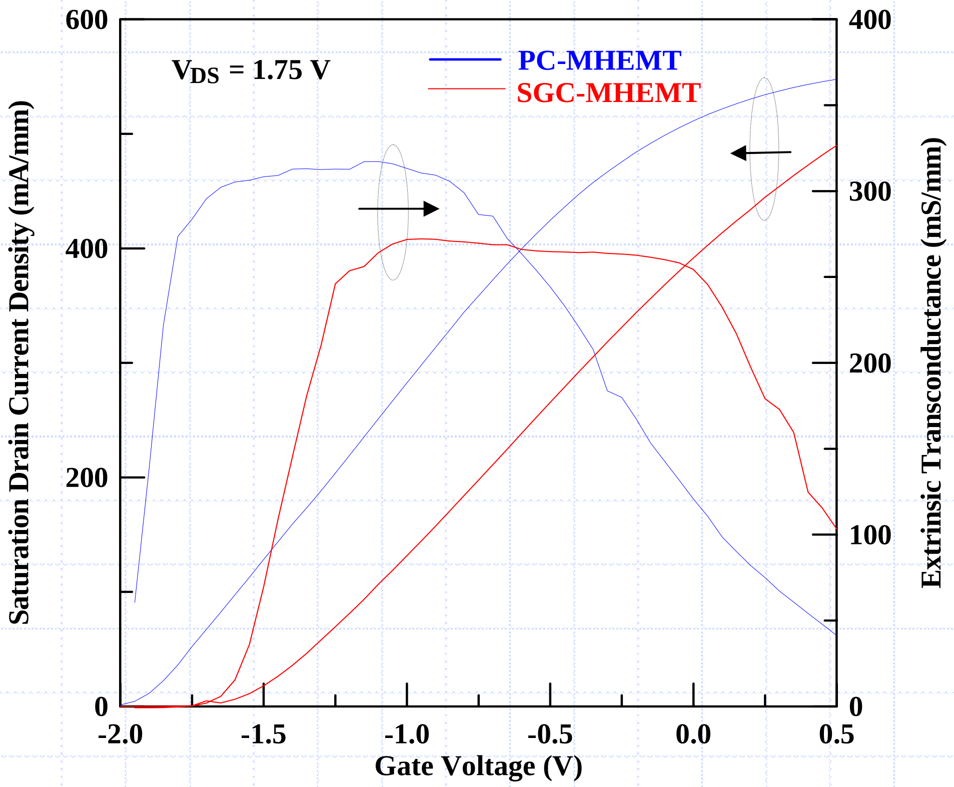

For PC-MHEMT:

- $g_{m,max}$ = 315 mS/mm
- I_{DSS0} = 511 mA/mm
- GVS = 1.05 V
- V_{th} = -1.93 V

For SGC-MHEMT:

- $g_{m,max}$ = 271 mS/mm
- I_{DSS0} = 391 mA/mm
- GVS = 1.3 V
- V_{th} = -1.68 V

II. Some Device Designs

- The threshold voltage (V_{th}) can be estimated by :

$$V_{th} = \frac{\phi_B}{q} - \frac{\Delta E_C}{q} - \frac{qN_d d_d}{\varepsilon}$$

where

$d_d = 25$ nm

$\varepsilon = 12 \times 8.85 \times 10^{-14}$ F/cm.

$N_d = 4.14 \times 10^{12}$ cm^{-2} (PC-MEHMT)

3.81×10^{12} cm^{-2} (SGC-MHEMT)

$\Delta E_C = 0.78$ eV (PC-MHEMT)

0.72 eV (SGC-MHEMT)

$\Phi_B = 0.51$ eV

V_{th} was calculated to be -1.84 V (PC-MHEMT) & -1.64 V (SGC-MHEMT).

Consistent expectations !!

II. Some Device Designs

Two-terminal gate-to-drain breakdown characteristics:

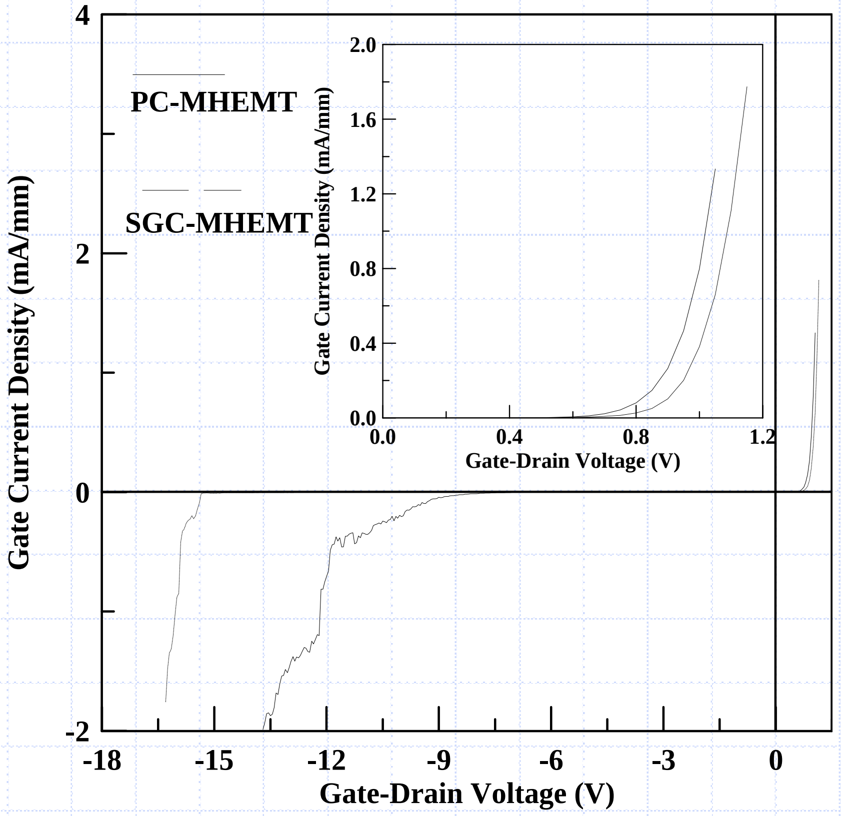

For PC-MHEMT:

- ***BV_{GD}* = -12.2 V**
- ***V_{on}* = 1.02 V**

For SGC-MHEMT:

- ***BV_{GD}* = -16.05 V**
- ***V_{on}* = 1 .1 V**

due to 2DEG location farther from gate electrode

II. *Some Device Designs*

- **Off-state breakdown characteristics:**
  by drain-current injection technique (*IEEE TED*, **40**, 1558, 1993.)

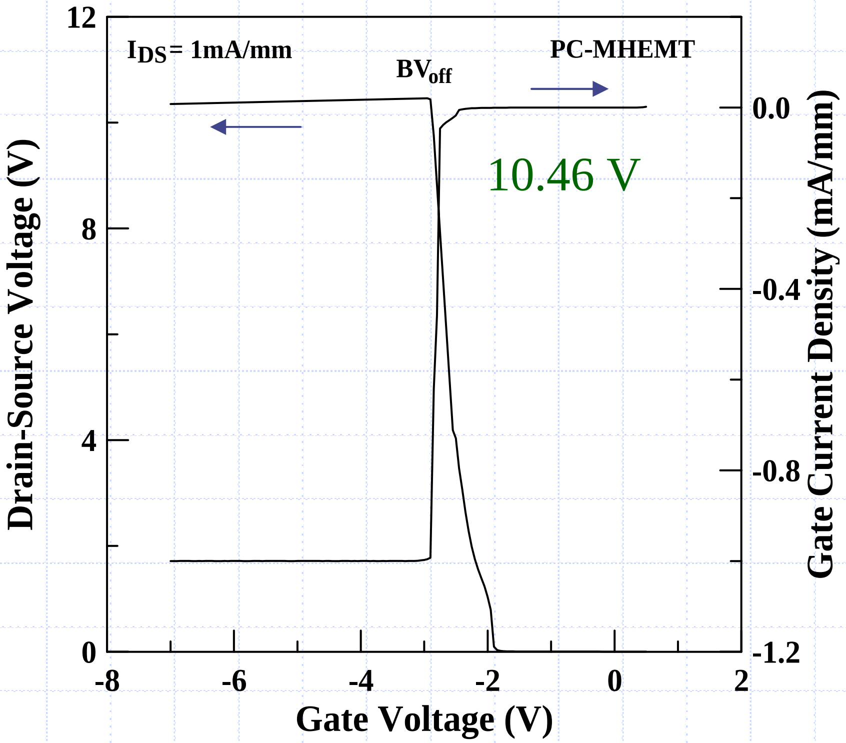

PC-MHEMT

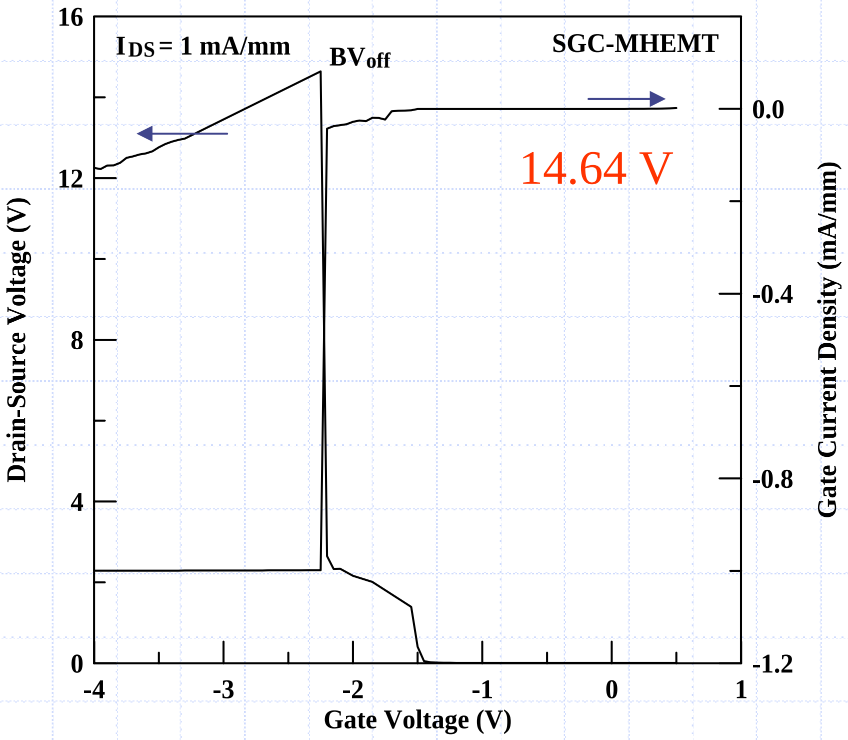

SGC-MHEMT

II. Some Device Designs

- **On-state breakdown characteristics :**

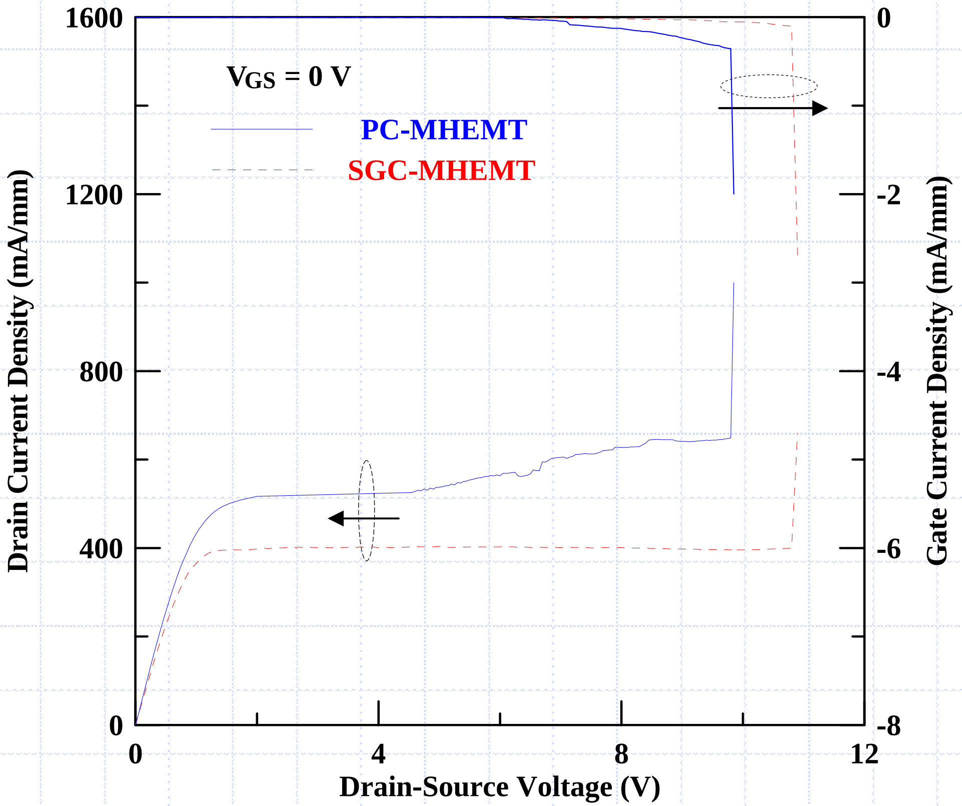

For PC-MHEMT:

BV_{on} = 9.85 V

For SGC-MHEMT:

BV_{on} = 10.9 V

II. *Some Device Designs*

- I_G vs. V_{GS} at increased V_{DS} :

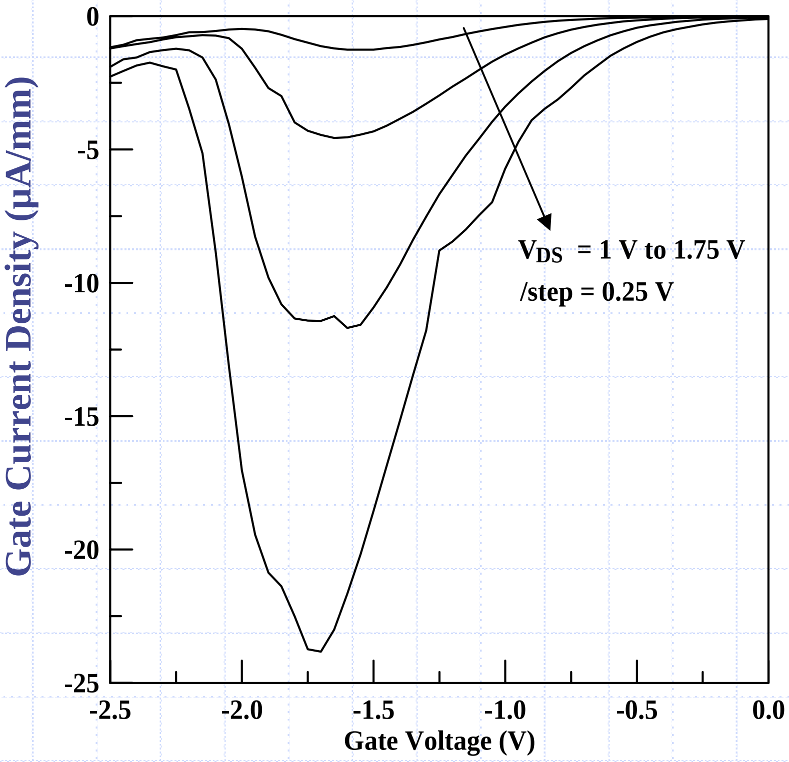

PC-MHEMT

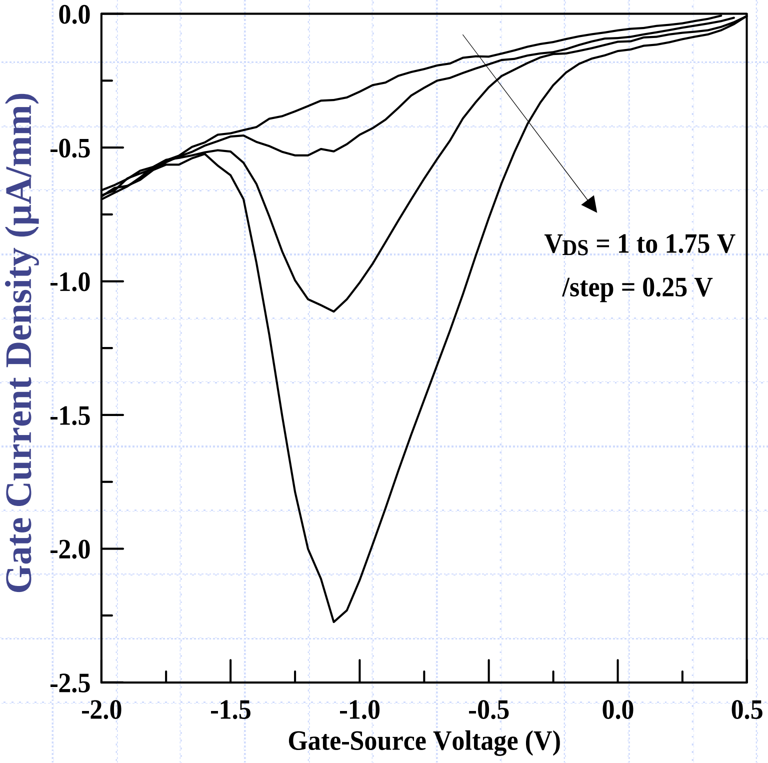

SGC-MHEMT

II. Some Device Designs

- **DC characteristics for PC-MHEMT and SGC-MHEMT:**

DC Characteristics	PC-MHEMT	SGC-MHEMT
I_{DSS0} (mA/mm)	511	391
$g_{m,max}$ (mS/mm)	315	271
V_{th} (V)	-1.93	-1.68
g_d (mS/mm)	13.5	11
A_V	23.2	24.6
GVS (V)	1.05	1.3
V_{on} (V)	1.02	1.1
BV_{GD} (V)	-12.2	-16.05
$BV_{DS, off}$ (V)	10.46	14.64
BV_{on} (V)	9.85	10.9
$I_{G,P}$ (μA/mm)	23.83	2.27

II. Some Device Designs

High-frequency characteristics:

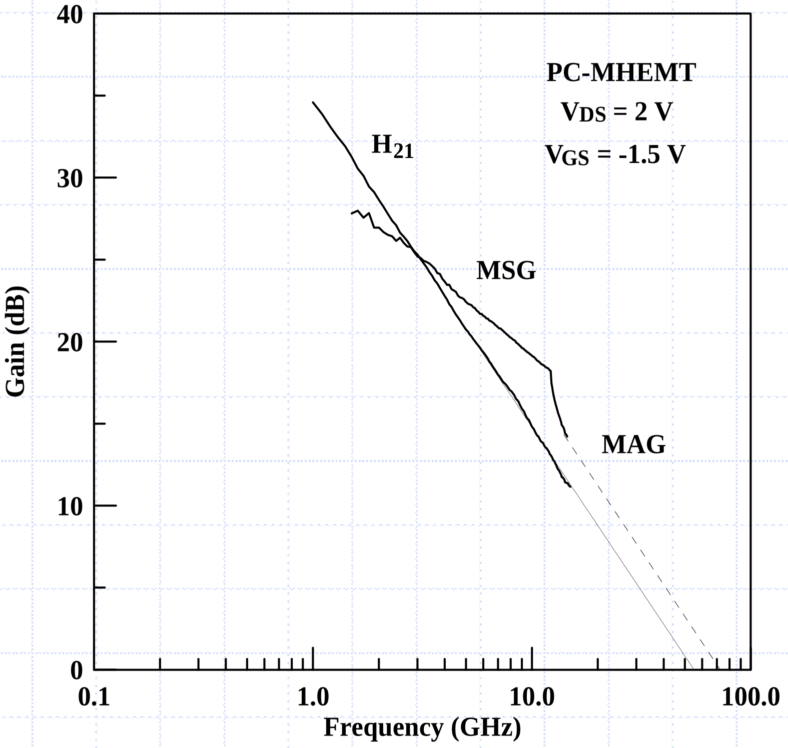

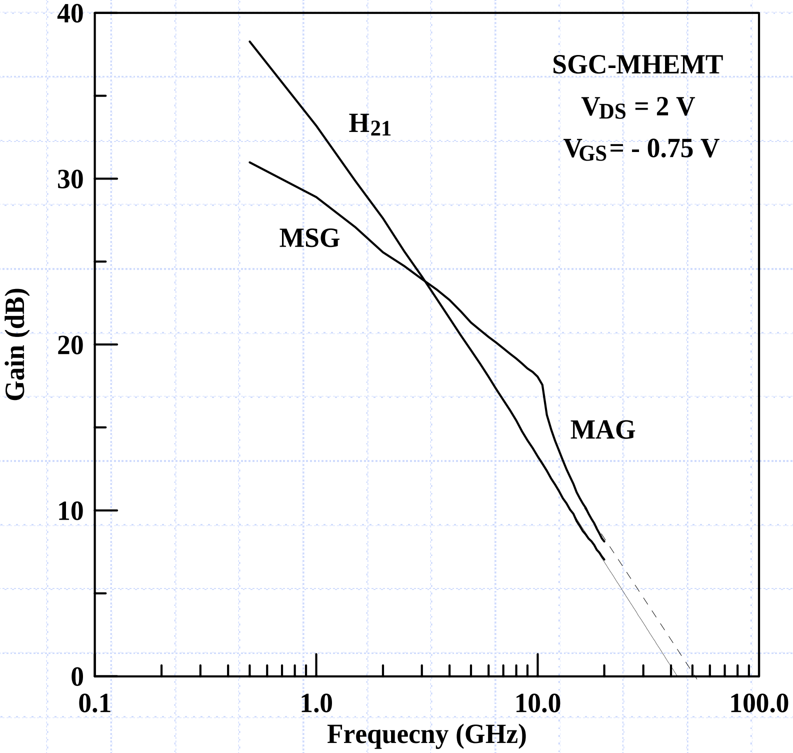

f_T = 55.4 GHz; f_{max} = 77.5 GHz

f_T = 42.8 GHz; f_{max} = 50.8 GHz

II. Some Device Designs

f_T and f_{max} vs. V_{GS} :

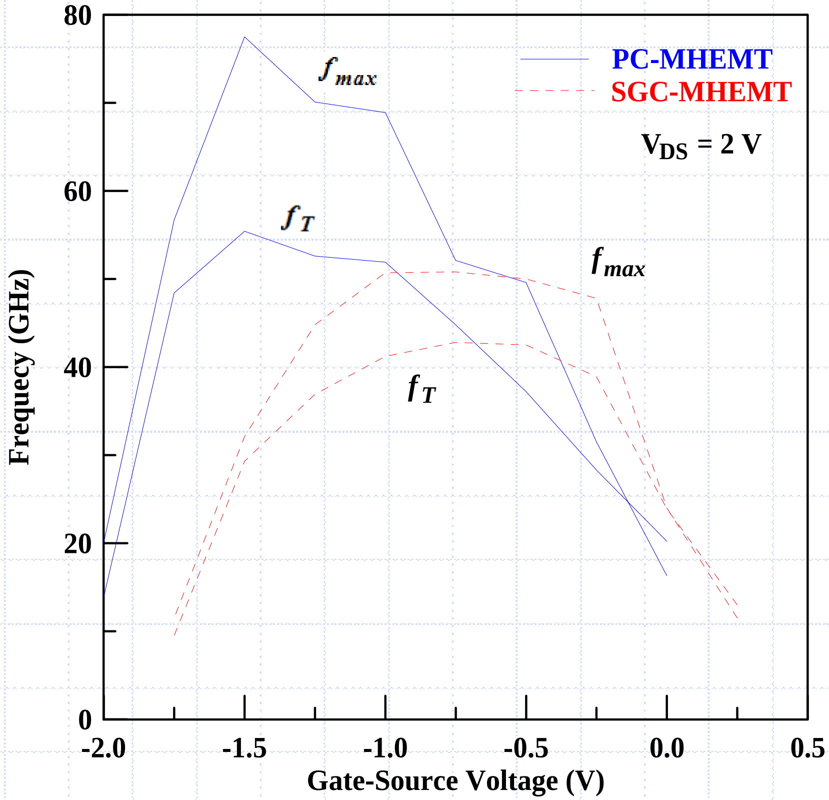

For PC-MHEMT:

- Higher f_T and f_{max} peak performances :

  $f_T = 55.4$ GHz; $f_{max} = 77.5$ GHz

$$f_T \approx \frac{g_m}{2\pi C_{gs}} \qquad f_{\max} \approx \frac{f_T}{2\sqrt{R_i g_d}}$$

For SGC-MHEMT:

- Wider constant frequency plateau :

  $V_{GS} = -1.25 \sim -0.25$ V

II. Some Device Designs

Power characteristics:

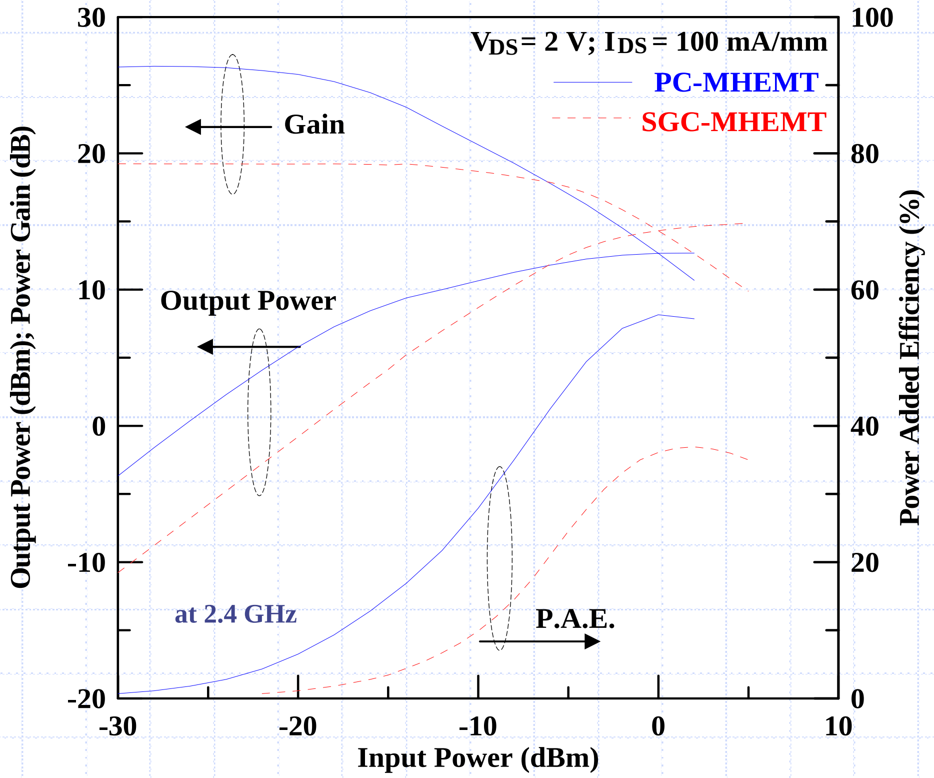

For PC-MHEMT:

- P_{out} = 12.6 dBm
- G_s = 26.3 dB
- PAE = 56 %

For SGC-MHEMT:

- P_{out} = 14.9 dBm
- G_s = 19.2 dB
- PAE = 37 %

- Suitable for high power application!!

II. Some Device Designs

Noise characteristics:

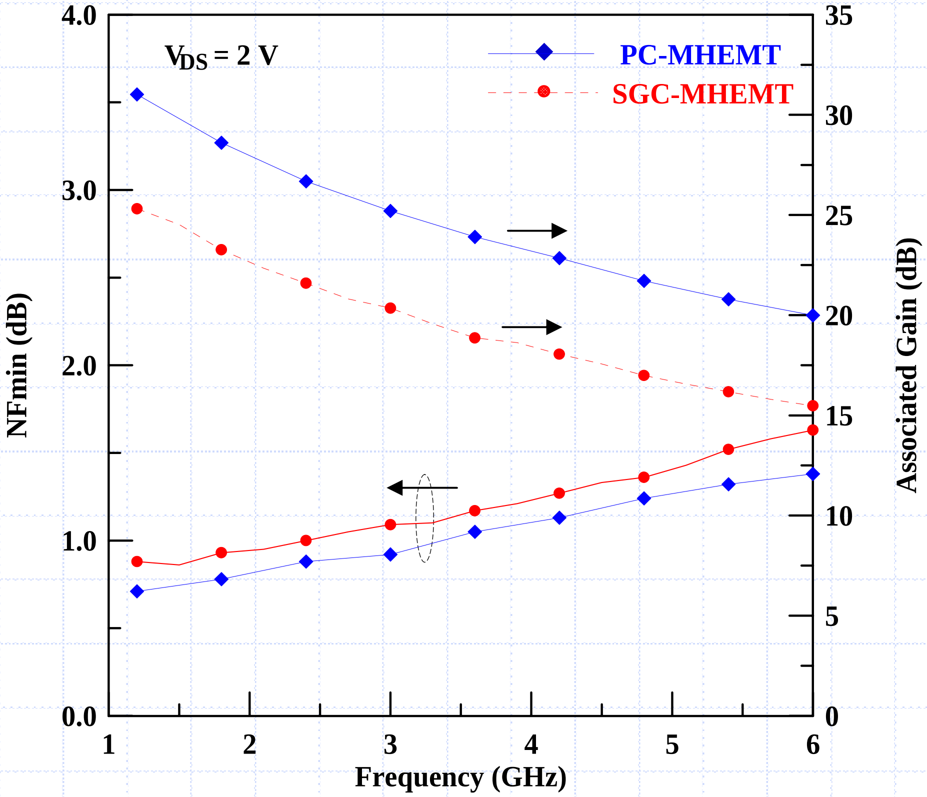

For PC-MHEMT at 2.4 GHz,
- ➢ NF_{min} = 0.88 dB.
- ➢ G_a = 26.68 dBm.

➢ Suitable for low-noise applications!!

For SGC-MHEMT at 2.4 GHz,
- ➢ NF_{min} = 0.95 dB.
- ➢ G_a = 21.59 dBm.

RF-Model Parameter Extraction:

- **Scattering parameters:**

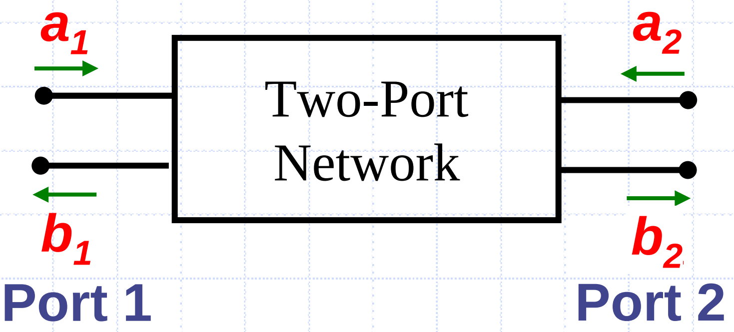

a_1 , a_2 : incident waves
b_1 , b_2 : reflected waves

$$b_1 = S_{11}a_1 + S_{12}a_2$$
$$b_2 = S_{21}a_1 + S_{22}a_2$$

$$S_{11} = \left.\frac{b_1}{a_1}\right|_{a_2=0}$$ Input Reflection Coefficient

$$S_{21} = \left.\frac{b_2}{a_1}\right|_{a_2=0}$$ Forward Transmission Coefficient

$$S_{12} = \left.\frac{b_1}{a_2}\right|_{a_1=0}$$ Reverse Transmission Coefficient

$$S_{22} = \left.\frac{b_2}{a_2}\right|_{a_1=0}$$ Output Reflection Coefficient

RF-Model Parameter Extraction:

- **Small-signal RF-model of HEMTs:**

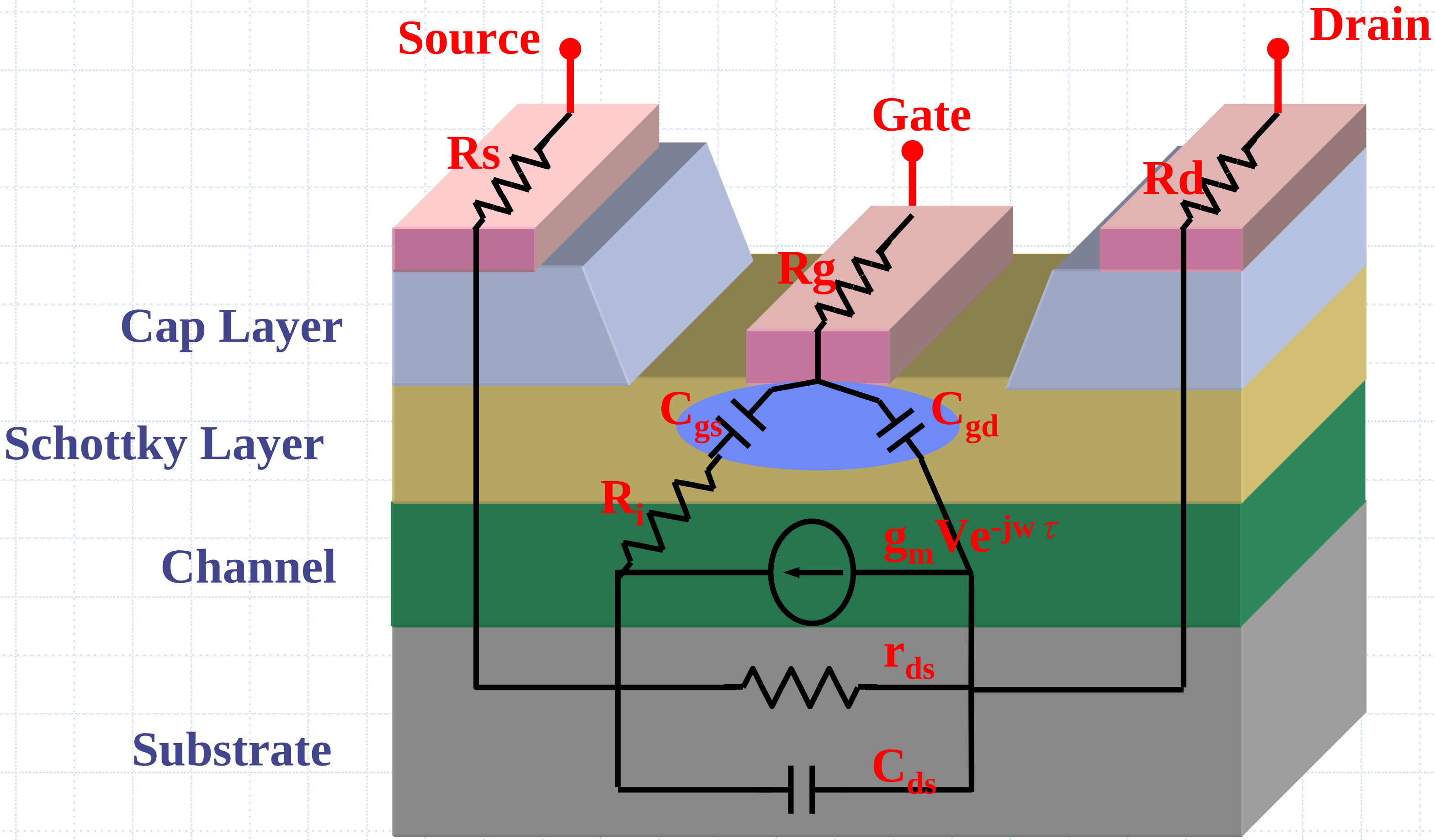

RF-Model Parameter Extraction:

- **Small-signal equivalent circuit:**

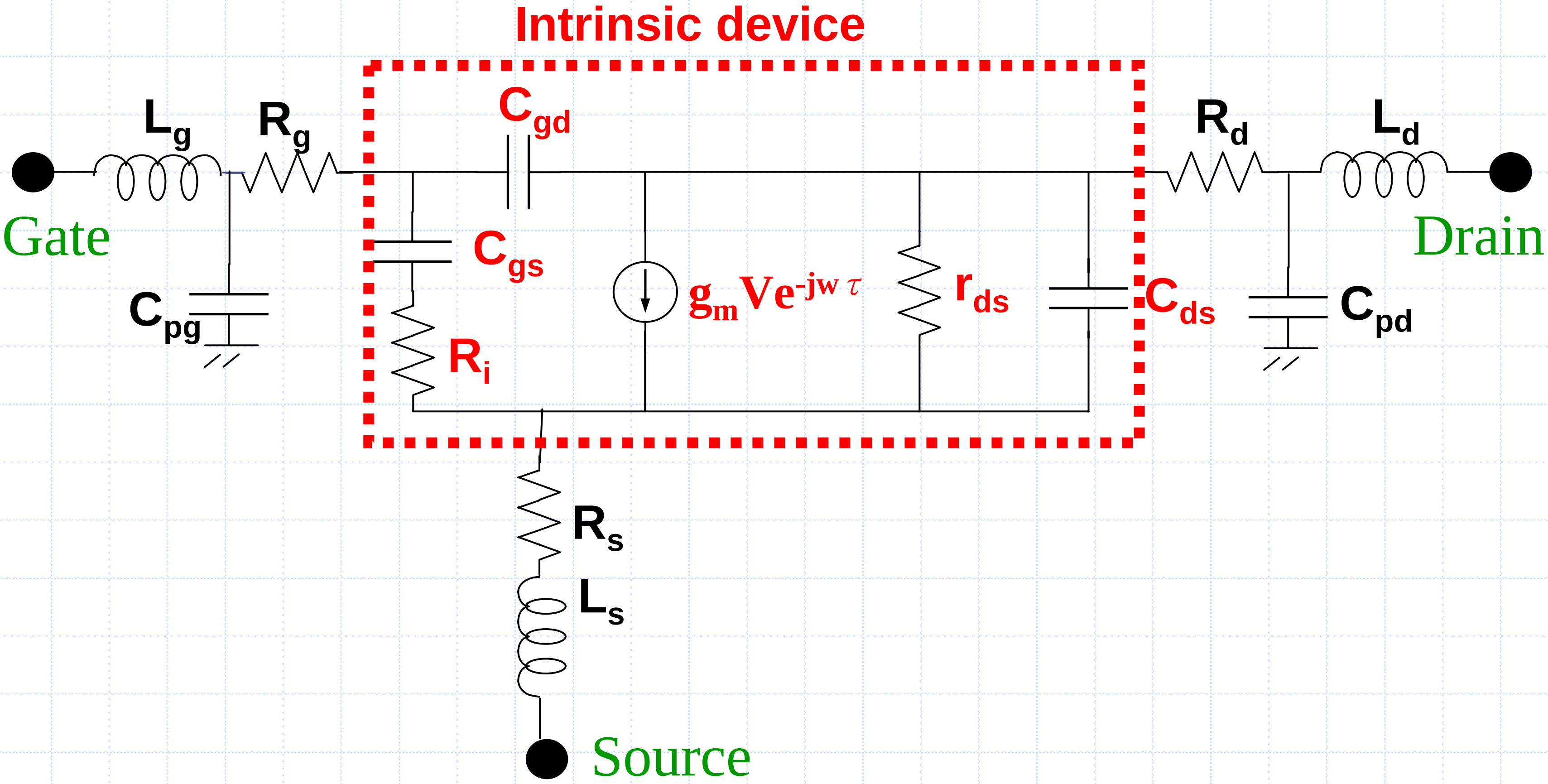

RF-Model Parameter Extraction:

- **De-embedding algorithms:**

$$\begin{bmatrix} S_{11} & S_{12} \\ S_{21} & S_{22} \end{bmatrix}$$

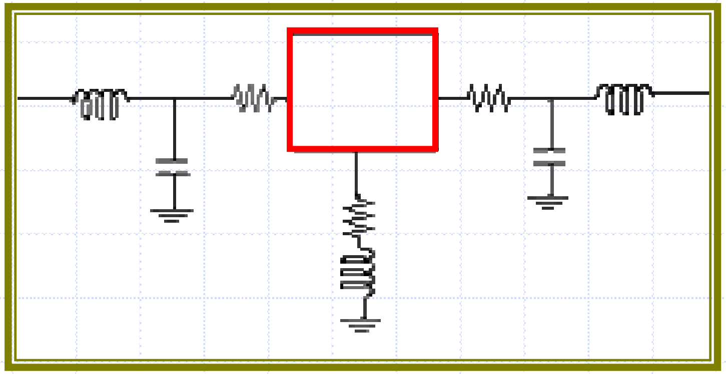

$$\begin{bmatrix} Z_{11}-R_s-R_g-jwL_s & Z_{12}-R_s-jwL_s \\ Z_{21}-R_s-jwL_s & Z_{22}-R_s-R_d-jwL_s \end{bmatrix}$$

$$\begin{bmatrix} Z_{11}-jwL_g & Z_{12} \\ Z_{21} & Z_{22}-jwL_d \end{bmatrix}$$

$$\begin{bmatrix} Y_{11}-jwC_{pg} & Y_{12} \\ Y_{21} & Y_{22}-jwC_{pd} \end{bmatrix}$$

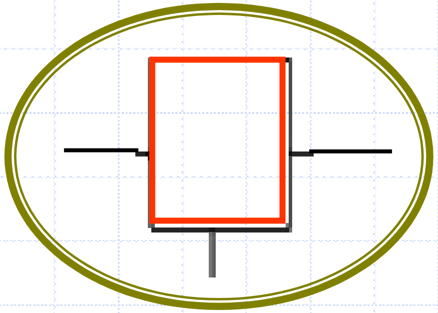

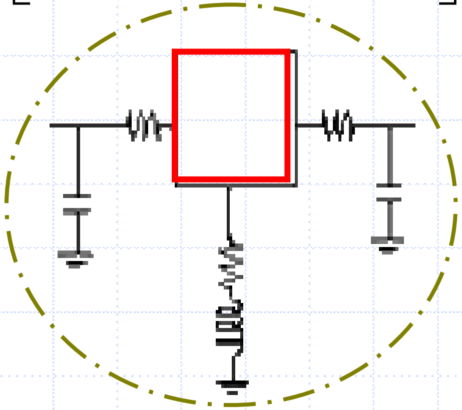

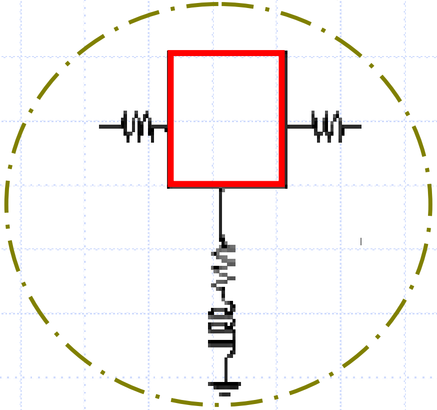

$Z \rightarrow Y$

RF-Model Parameter Extraction:

- **Cold Model:**
  - ⇨ **All S-parameter measurement were carrier out at V_{DS} = 0V with $V_{GS} > V_p$**

$$Z11 = R_s + R_g + \frac{R_c}{3} + \frac{nkT}{qI_g} + j\omega\left(L_s + L_g\right)$$

$$Z12 = Z21 = R_s + \frac{R_c}{2} + j\omega L_s$$

$$Z22 = R_s + R_d + R_c + j\omega\left(L_s + L_d\right)$$

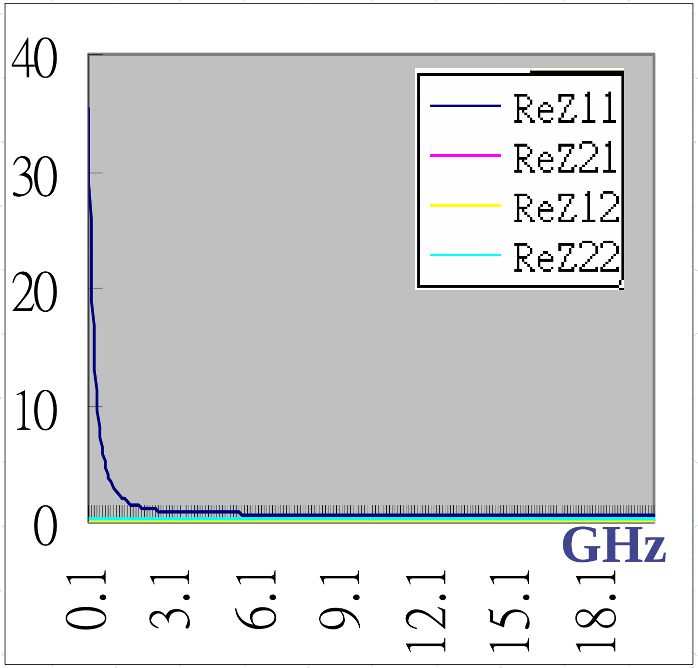

Rs
Rd
Rg

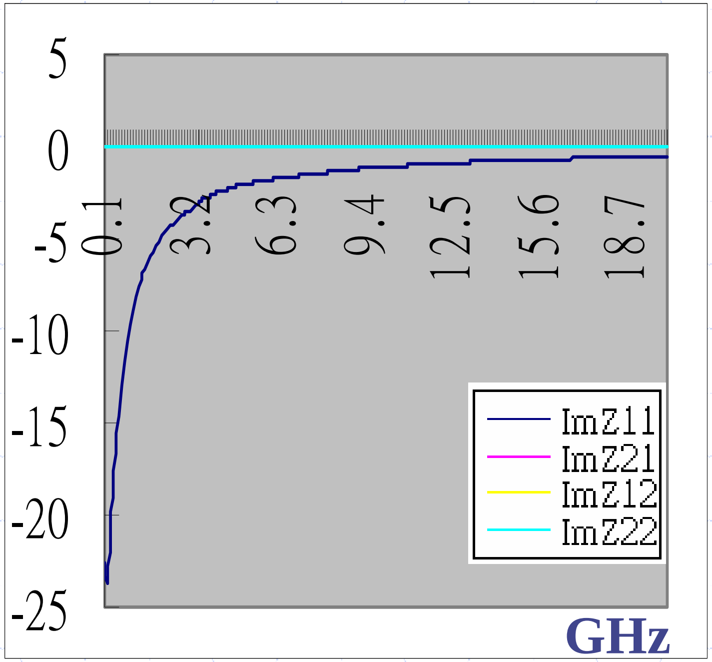

Ls
Ld
Lg

RF-Model Parameter Extraction:

- **S-parameter measurement were carried out at $V_{DS} = 0V$ when $V_{GS} < V_p$**

$$\mathrm{Im}(Y_{11}) = j\omega(C_{pg} + 2C_b)$$
$$\mathrm{Im}(Y_{12}) = \mathrm{Im}(Y_{21}) = -j\omega C_b$$
$$\mathrm{Im}(Y_{22}) = j\omega(C_b + C_{pd})$$

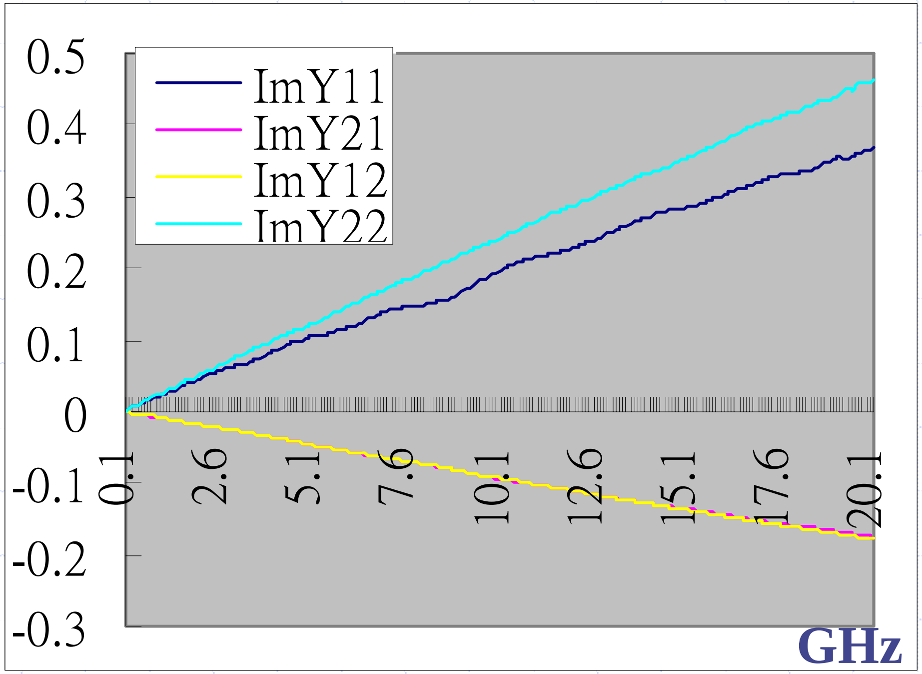

C_{pg}

C_b

C_{pd}

RF-Model Parameter Extraction:

➢ Theoretical analysis: Intrinsic

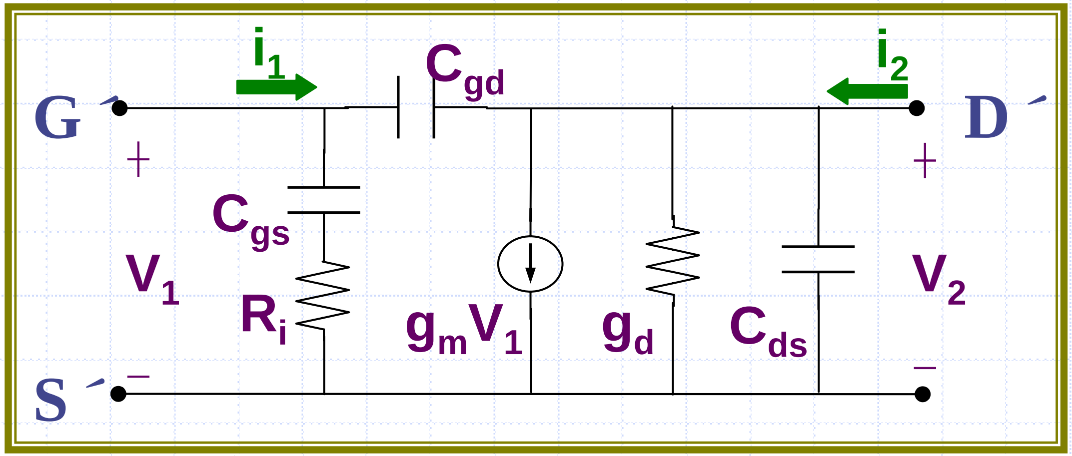

$$i_1 = y_{11}V_1 + y_{12}V_2$$

$$i_2 = y_{21}V_1 + y_{22}V_2$$

$$y_{11} = \left.\frac{i_1}{V_1}\right|_{V_2} = 0(D' - S'\ Short)$$

$$y_{12} = \left.\frac{i_1}{V_2}\right|_{V_1} = 0(G' - S'\ Short)$$

$$y_{21} = \left.\frac{i_2}{V_1}\right|_{V_2} = 0(D' - S'\ Short)$$

$$y_{22} = \left.\frac{i_2}{V_2}\right|_{V_1} = 0(G' - S'\ Short)$$

$$y_{11} = \frac{R_i C_{gs}{}^2 w^2}{1 + w^2 C_{gs}{}^2 R_i{}^2} + jw\left(\frac{C_{gs}}{D} + C_{gd}\right)$$

$$y_{12} = -jwC_{gd}$$

$$y_{21} = \frac{g_m \exp(-jw\tau)}{1 + jR_i C_{gs} w} - jwC_{gd}$$

$$y_{22} = g_d + jw(C_{ds} + C_{gd})$$

RF-Model Parameter Extraction:

- **At low frequency:**

$$y_{11} = R_i C_{gs}^2 \omega^2 + j\omega\left(C_{gs} + C_{gd}\right)$$

$$y_{12} = -j\omega C_{gd}$$

$$y_{21} = g_m - j\omega\left(C_{gd} + g_m\left(R_i C_{gs} + \tau\right)\right)$$

$$y_{22} = g_d + j\omega\left(C_{ds} + C_{gd}\right)$$

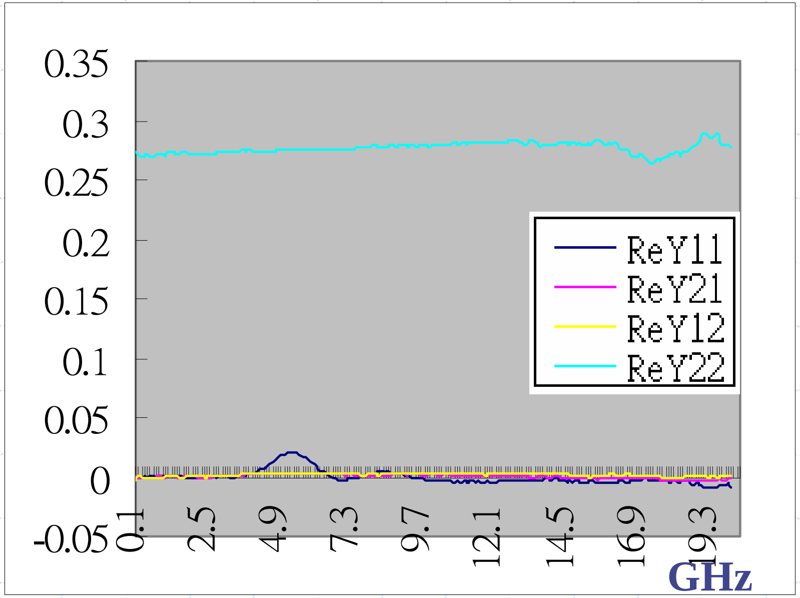

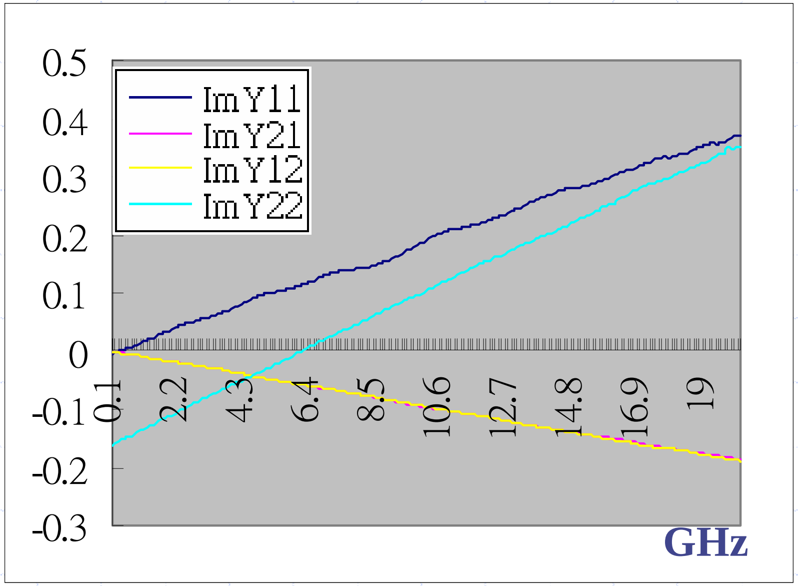

ReY ⇨ **R_i, g_m, g_d**

ImY ⇨ **C_{gs}, C_{gd}, C_{ds}, τ**

RF-Model Parameter Extraction:

- **Complete extracted RF model:**

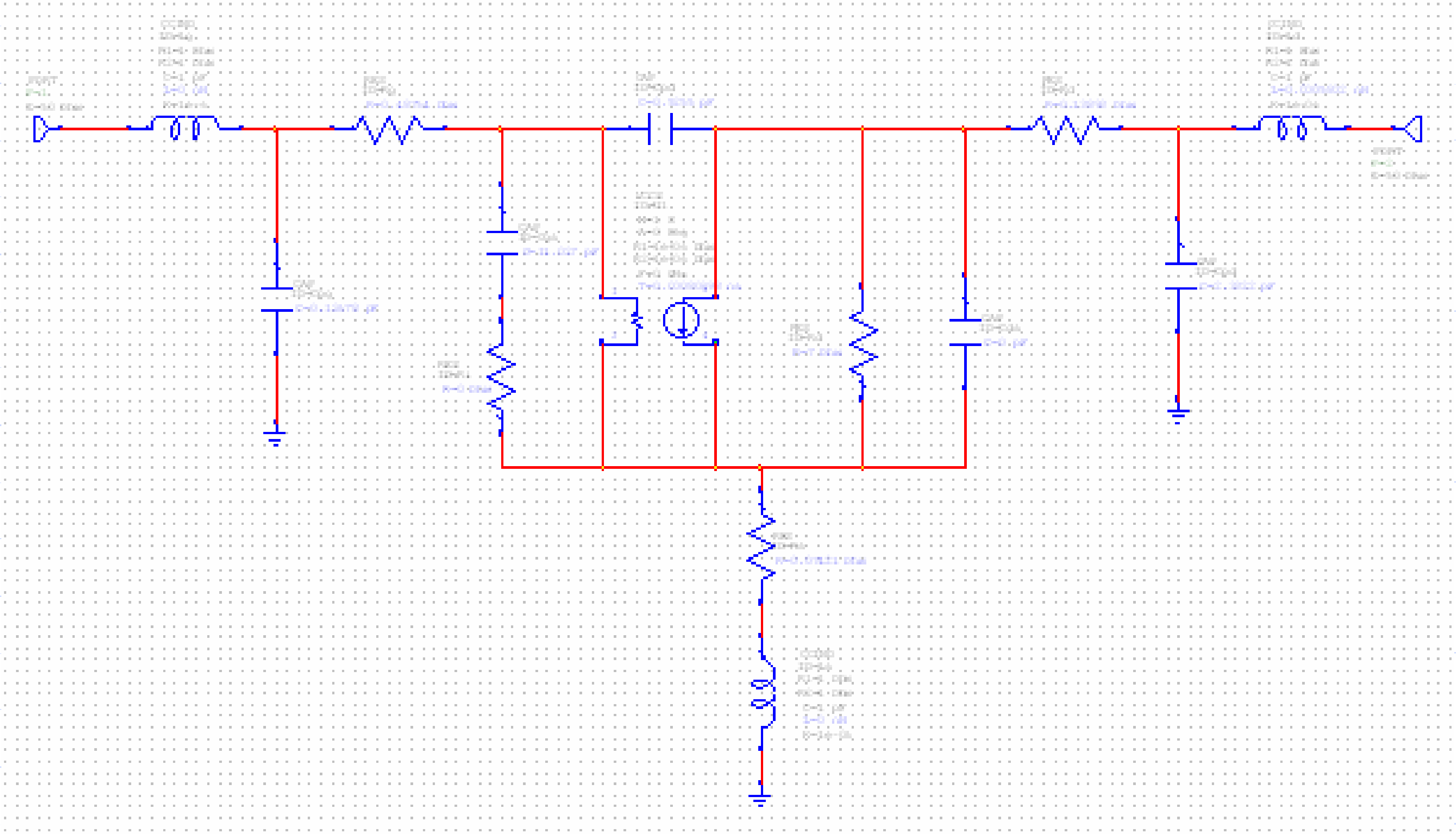

RF-Model Parameter Extraction:

Small-Signal Parameters	PC-MHEMT	SGC-MHEMT
Gate Inductance, L_g (nH),	0.012	0.011
Drain Inductance, L_d (nH)	0.09	0.089
Source Inductance, L_s (nH)	0.013	0.008
Gate Resistance, R_g (Ω)	21.6	21.3
Drain Resistance, R_d (Ω)	10.1	13.7
Source Resistance, R_s (Ω)	4.7	4.4
Charging Resistance, R_i (Ω)	1.7	2.1
Output Resistance, R_{ds} (Ω)	343	433
Output Conductance, g_d (mS, mS/mm)	2.91 (14.58)	2.31 (11.55)
Intrinsic Transconductance, G_m (mS, mS/mm)	90 (450)	75 (375)
Transconductance Delay, T (ps)	1.4	1.6
Gate-Drain Capacitance, C_{gd} (pF)	0.0083	0.0126
Gate-Source Capacitance, C_{gs} (pF)	0.24	0.23
Drain-Source Capacitance, C_{ds} (pF)	0.0615	0.0511

RF-Model Parameter Extraction:

S-Parameter for PC-MHEMT:

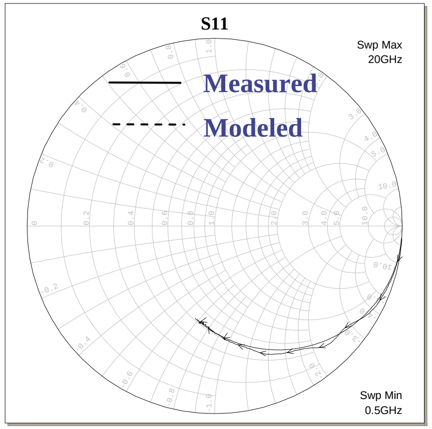

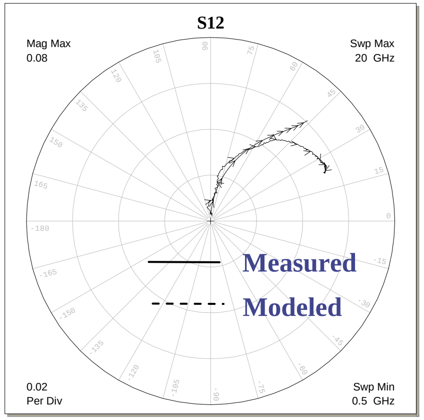

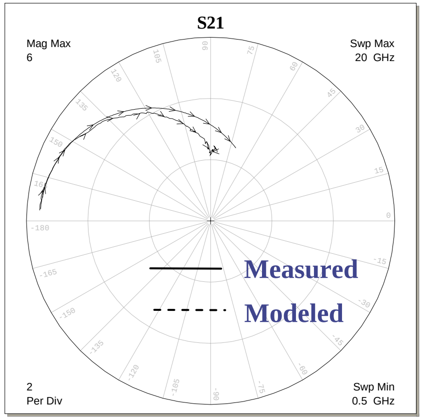

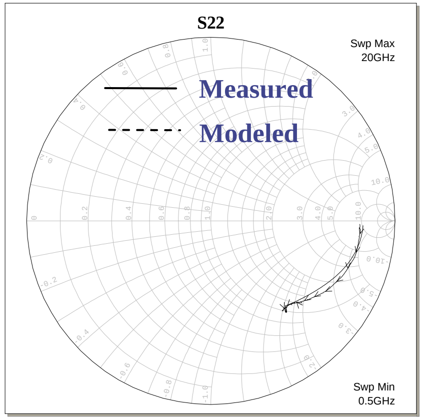

RF-Model Parameter Extraction:

S-Parameter for SGC-MHEMT:

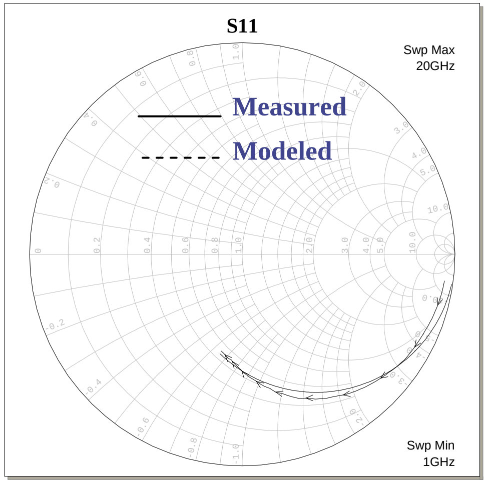

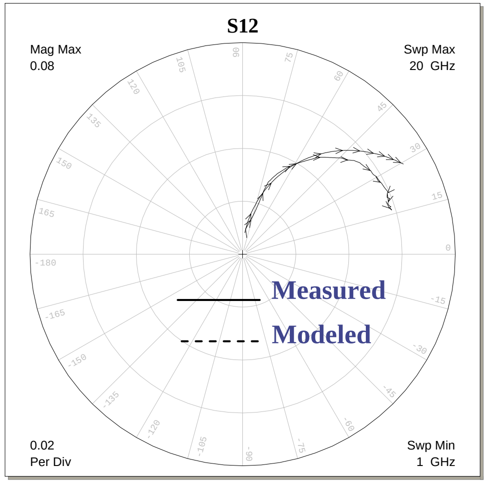

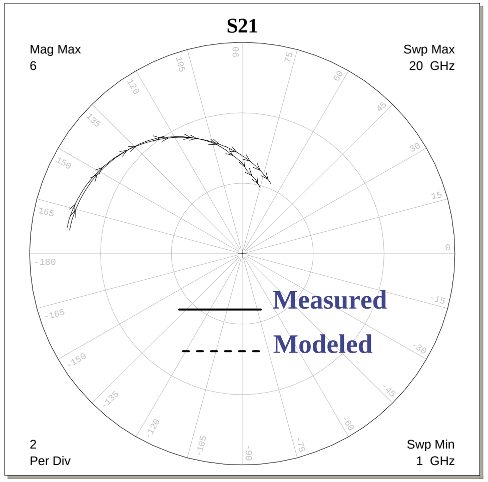

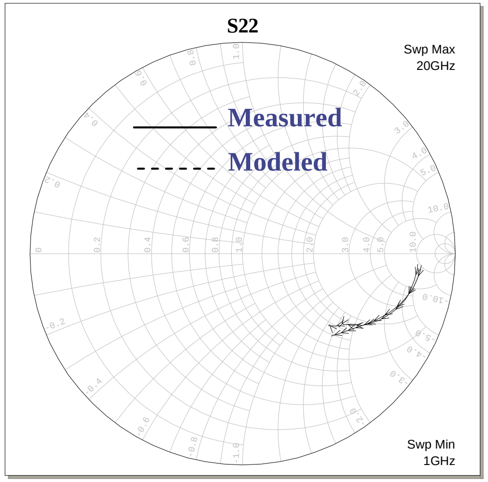

RF-Model Parameter Extraction:

- **Verifications with measurement results:**

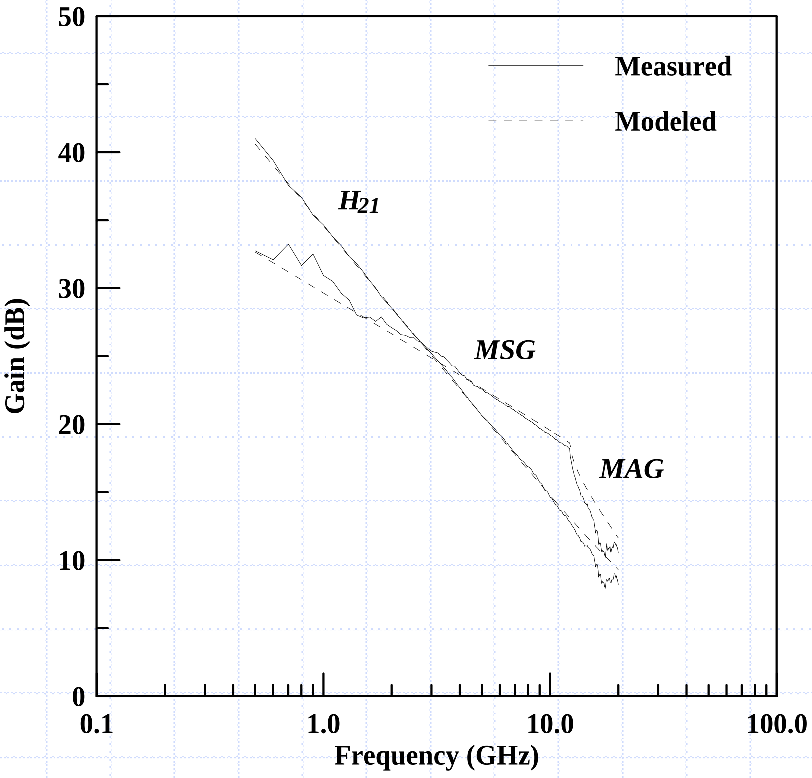

■ **PC-MHEMT**

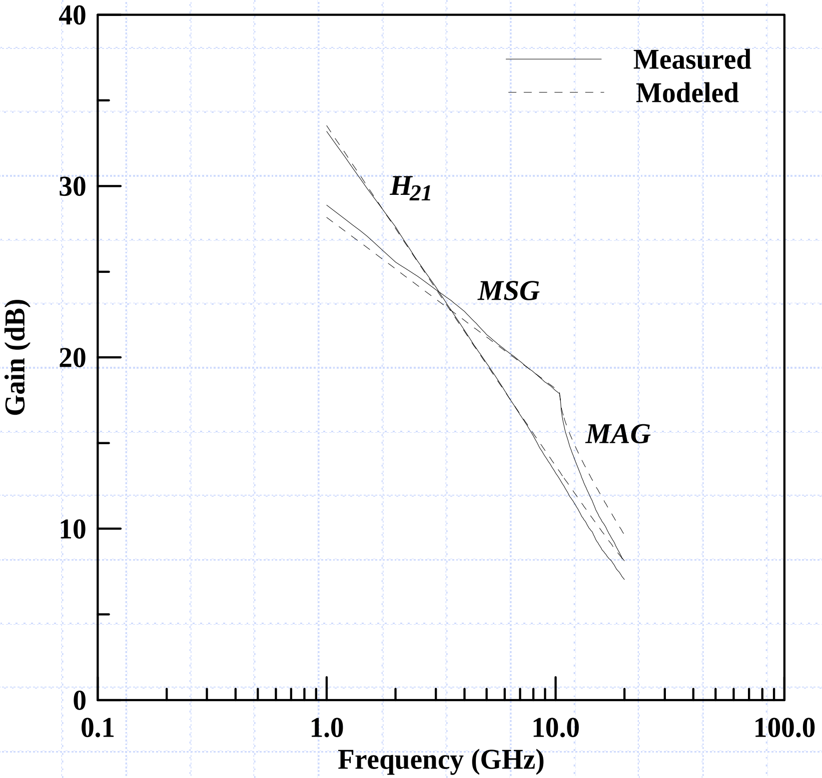

■ **SGC-MHEMT**

Gate-Alloys-Related Kink Effects

- **Schematic cross section of δ-doped $In_{0.45}Al_{0.55}As/In_{0.53}Ga_{0.47}$ MHEMT**

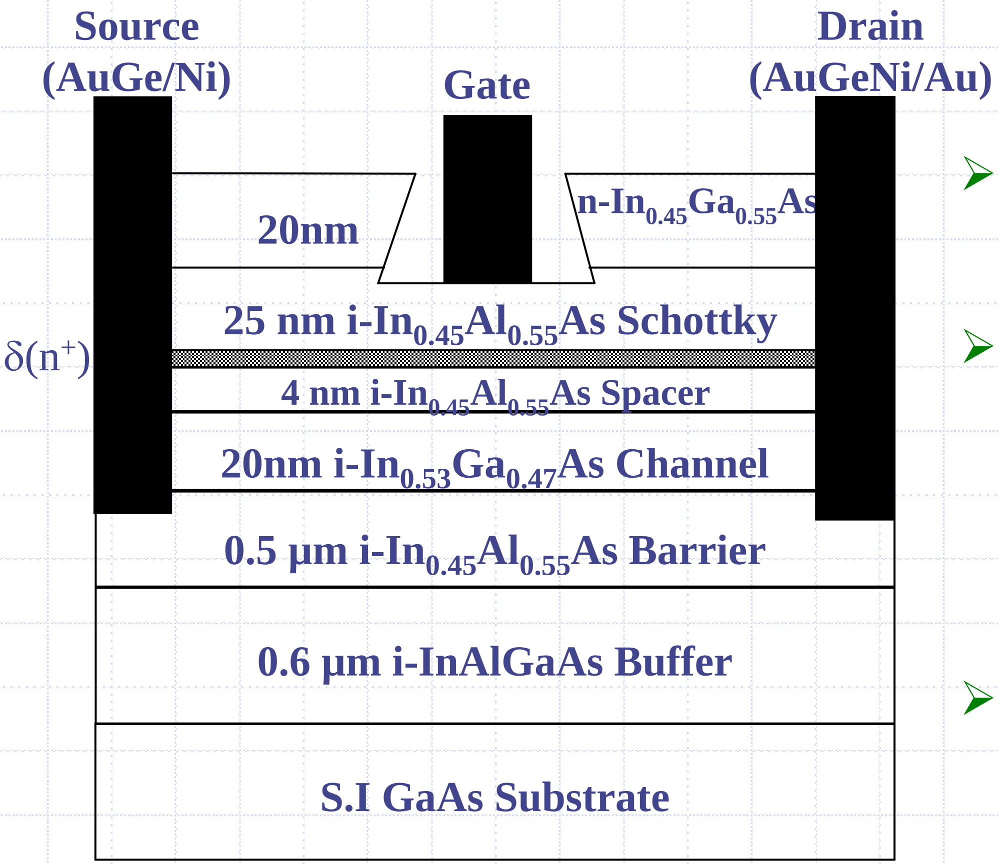
Source (AuGe/Ni)

Gate

Drain (AuGeNi/Au)

20nm

$n-In_{0.45}Ga_{0.55}As$

25 nm $i-In_{0.45}Al_{0.55}As$ Schottky

$\delta(n^+)$

4 nm $i-In_{0.45}Al_{0.55}As$ Spacer

20nm $i-In_{0.53}Ga_{0.47}As$ Channel

0.5 µm $i-In_{0.45}Al_{0.55}As$ Barrier

0.6 µm i-InAlGaAs Buffer

S.I GaAs Substrate

- **300K**
  mobility = 7658 $cm^2/V \cdot s$
  carrier concentration = 2.9×10^{12} cm^{-2}
- **77K**
  mobility = 30083 $cm^2/V \cdot s$
  carrier concentration = 3.6×10^{12} cm^{-2}

- **Gate dimension** : 1.2×200 μm^2

Gate-Alloys-Related Kink Effects

- **Schematic band diagram of MHEMT with Au and Ni/Au gates:**

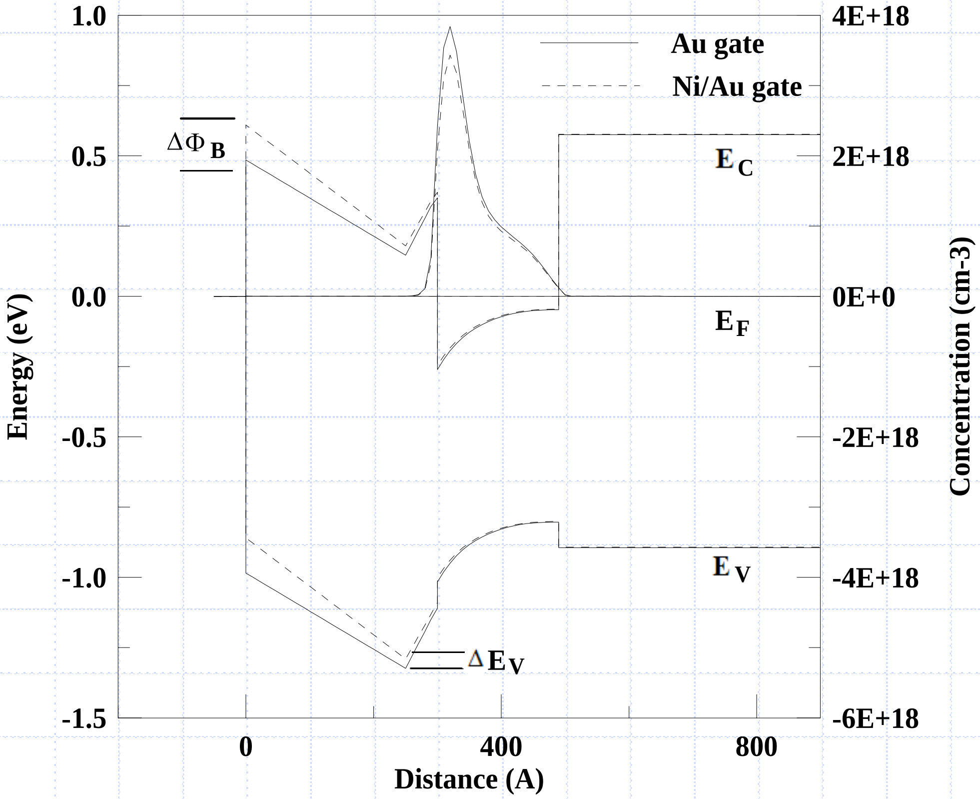

Gate-Alloys-Related Kink Effects

- **I-V characteristics with Au and Ni/Au gates:**

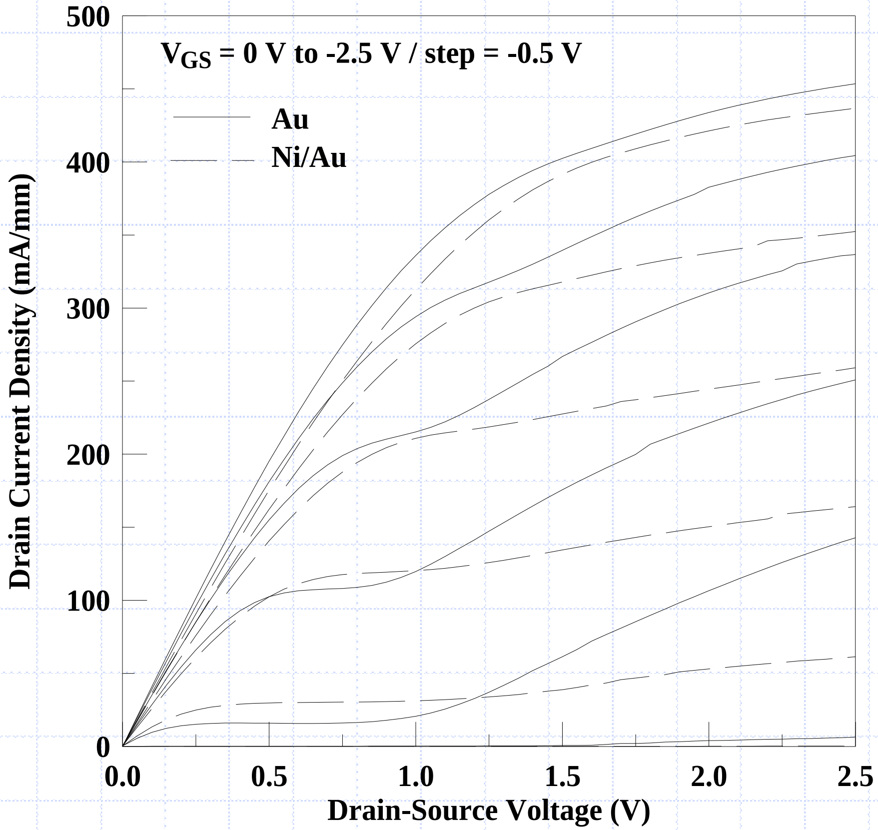

Gate-Alloys-Related Kink Effects

- g_m and I_{DSS} as a function V_{GS} :

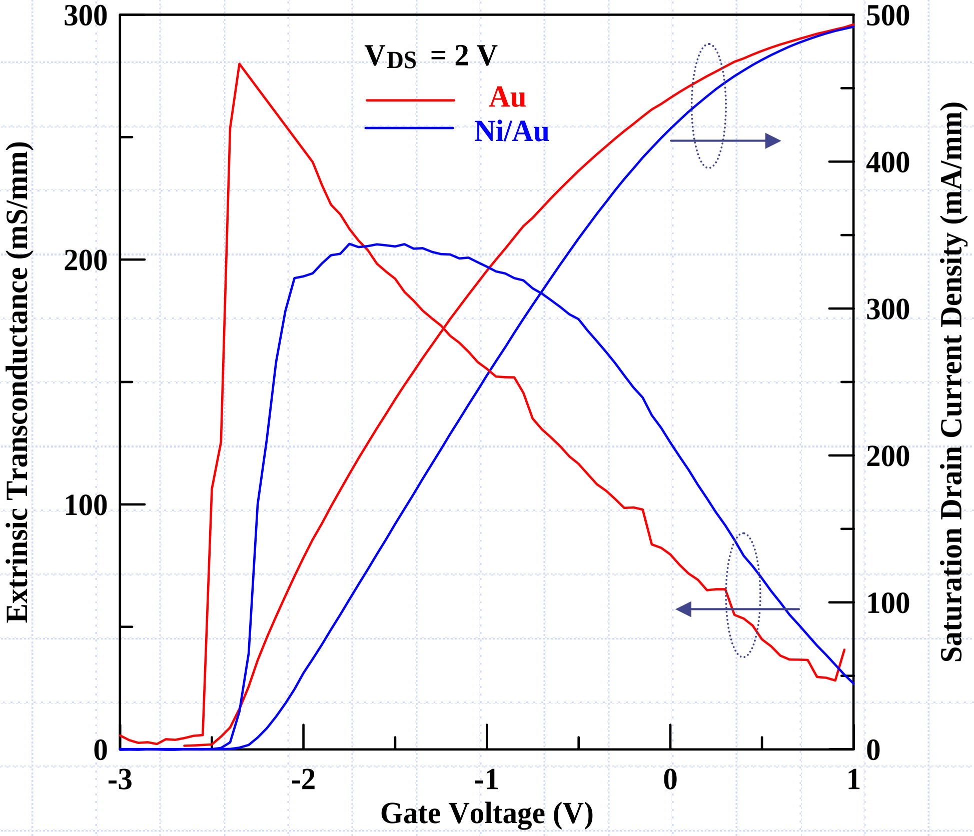

■ Au gate-metal

- $g_{m,\ max}$ = 280 mS/mm at V_{DS} = 2 V
- I_{DSS} = 433 mA/mm at V_{GS} = 0 V

■ Ni/Au gate-metal

- $g_{m,\ max}$ = 206 mS/mm at V_{DS} = 2 V
- I_{DSS} = 421 mA/mm at V_{GS} = 0V

Gate-Alloys-Related Kink Effects

- **Gate current density as a function of V_{GS} for various V_{DS} :**

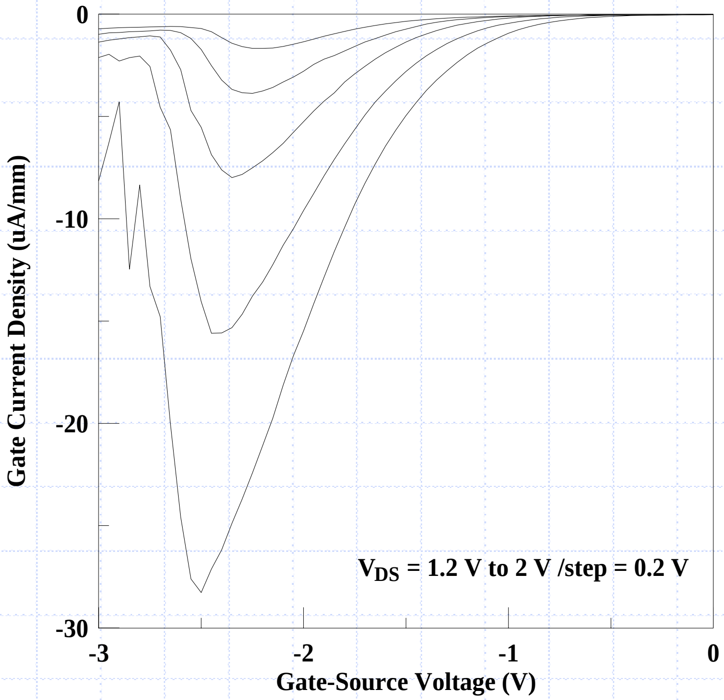

Au

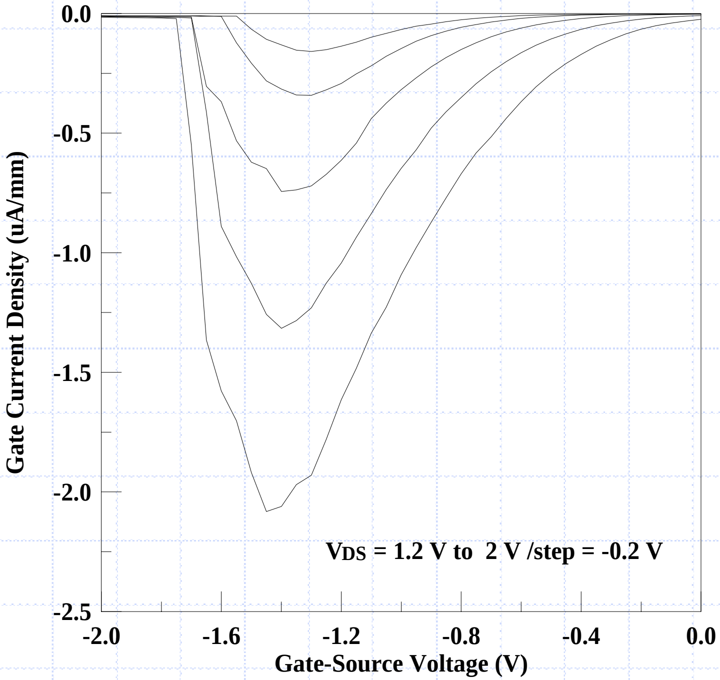

Ni/Au

Gate-Alloys-Related Kink Effects

- g_m, and g_d characteristics as a function of V_{DS} :

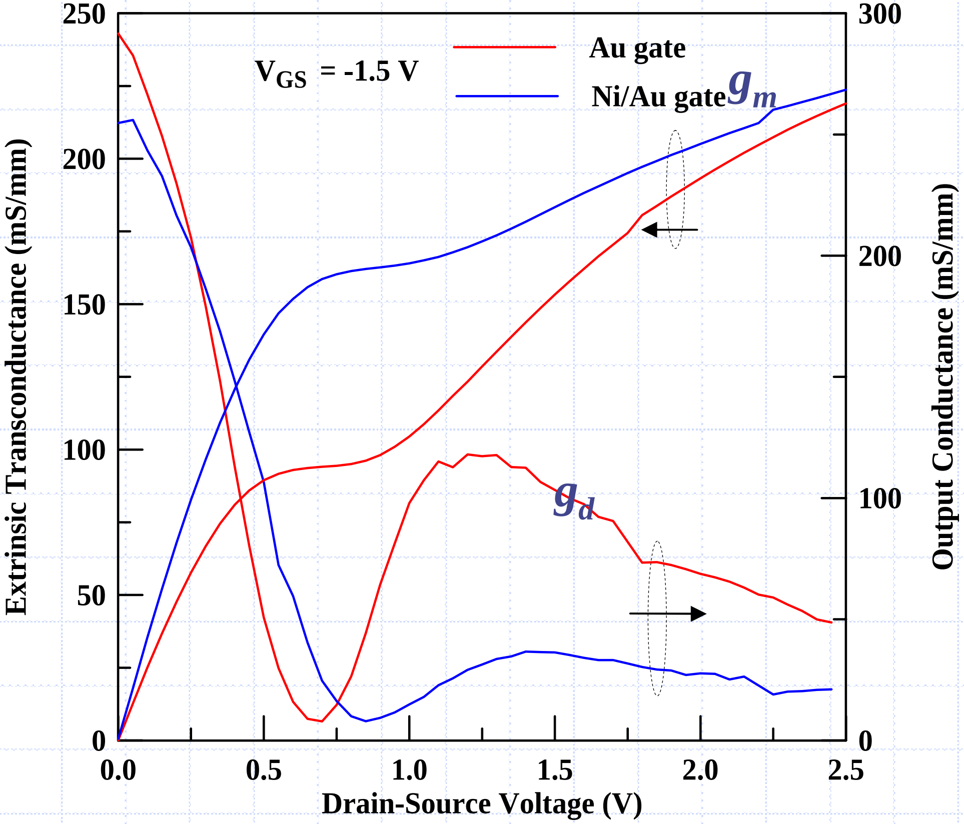

- at V_{DS} = 2 V and V_{GS} = - 1.5 V

- **Au gate-metal**
  - g_m = 193 mS/mm
  - g_d = 68.7 mS/mm
  - A_V = 2.81

- **Ni/Au gate-metal**
  - g_m = 204 mS/mm
  - g_d = 26.1 mS/mm
  - A_V = 7.83

Gate-Alloys-Related Kink Effects

- Comparisons of I_{DSS0}, $g_{m.max}$, $I_{G,\ peak}$, g_d, and A_v :

Gate Metal	Au	Ti/Au	Ni/Au	Pt/Au
I_{DSS} (mA/mm)	433	415	421	394
$g_{m,max}$ (mS/mm)	280	220	206	200
$I_{G,\ peak}$ (μA/mm) at $V_{DS} = 2$ V	28.3	14.5	2.1	2.2
g_d (mS/mm) $V_{DS} = 2$ V	68.7	27.6	26.1	18.1
A_v $V_{DS} = 2$ V	2.81	7.61	7.83	11.05

Gate-Alloys-Related Kink Effects

- **Two-terminal gate-drain characteristics :**

forward turn-on characteristics

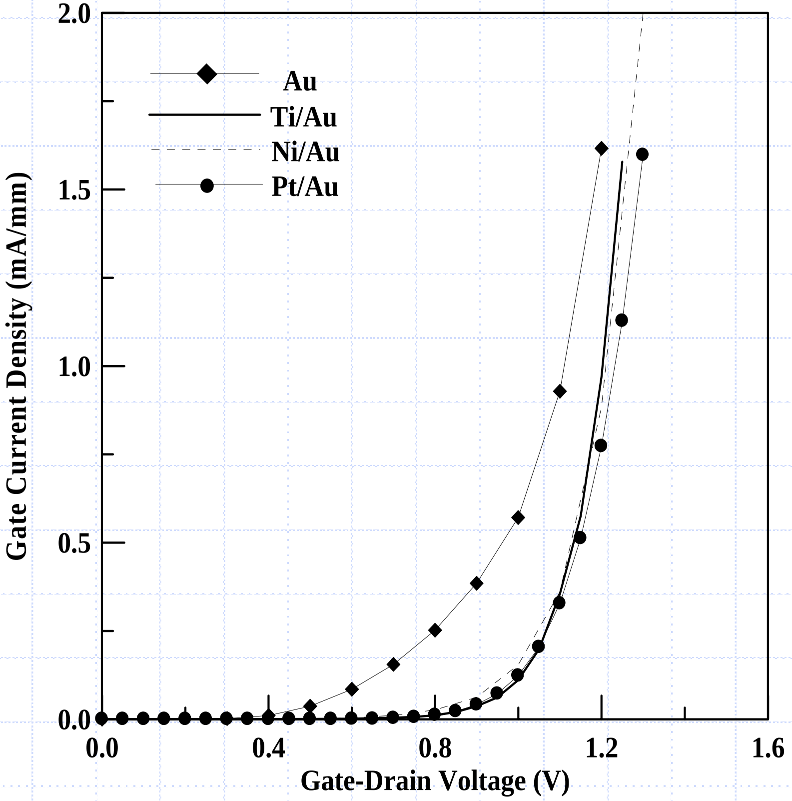

reverse breakdown characteristics

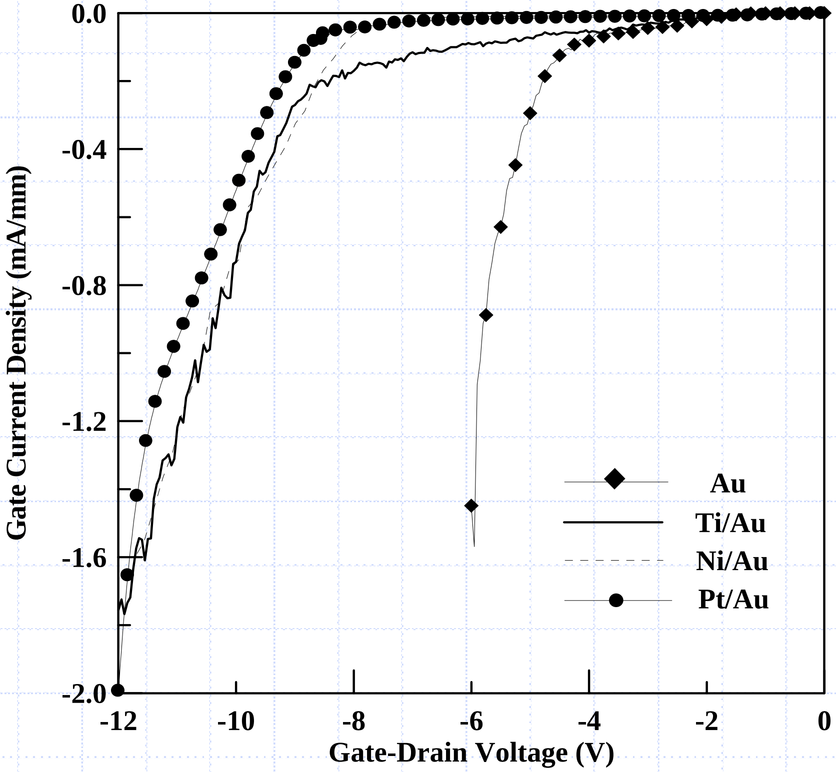

Gate-Alloys-Related Kink Effects

- **Comparisons of Φ_B, V_{on}, BV_{GD}, and V_{th} :**

Gate Metal	Au	Ti/Au	Ni/Au	Pt/Au
Φ_B (meV)	485	606	608	730
V_{on} (V)	1.11	1.20	1.21	1.23
BV_{GD} (V)	-5.8	-10.5	-10.6	-11
V_{th} (V)	-2.47	-2.24	-2.24	-1.95

Gate-Alloys-Related Kink Effects

Microwave characteristics:

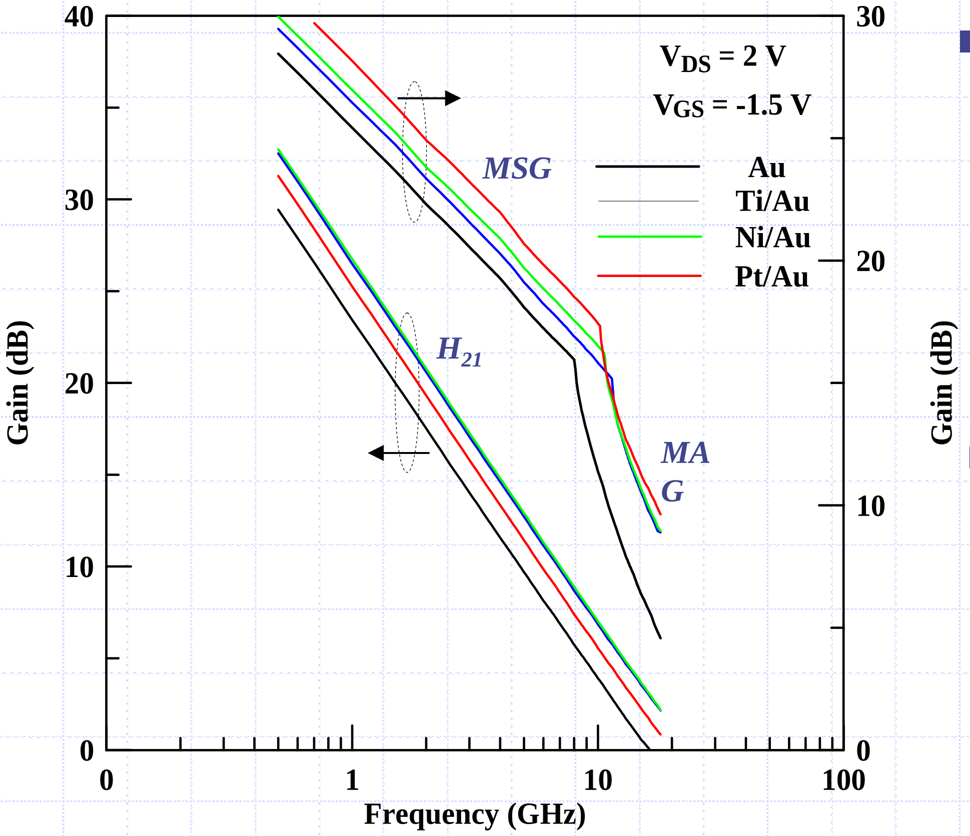

- f_T : Ni/Au = Ti/Au > Pt/Au >Au

$$f_T \approx \frac{g_m}{2\pi C_{gs}}$$

  - g_m are 193, 210, 204, and 200 mS/mm for Au, Ti/Au, Ni/Au and Pt/Au

- f_{max} : Pt/Au > Ni/Au > Ti/Au >Au

$$f_{\max} \approx \frac{f_T}{2\sqrt{R_i g_d}}$$

  - $\frac{f_T}{\sqrt{g_d}}$: 2.08, 4.53, 4.66, 4.75
  - for Au, Ti/Au, Ni/Au and Pt/Au

Gate-Alloys-Related Kink Effects

Power characteristics :

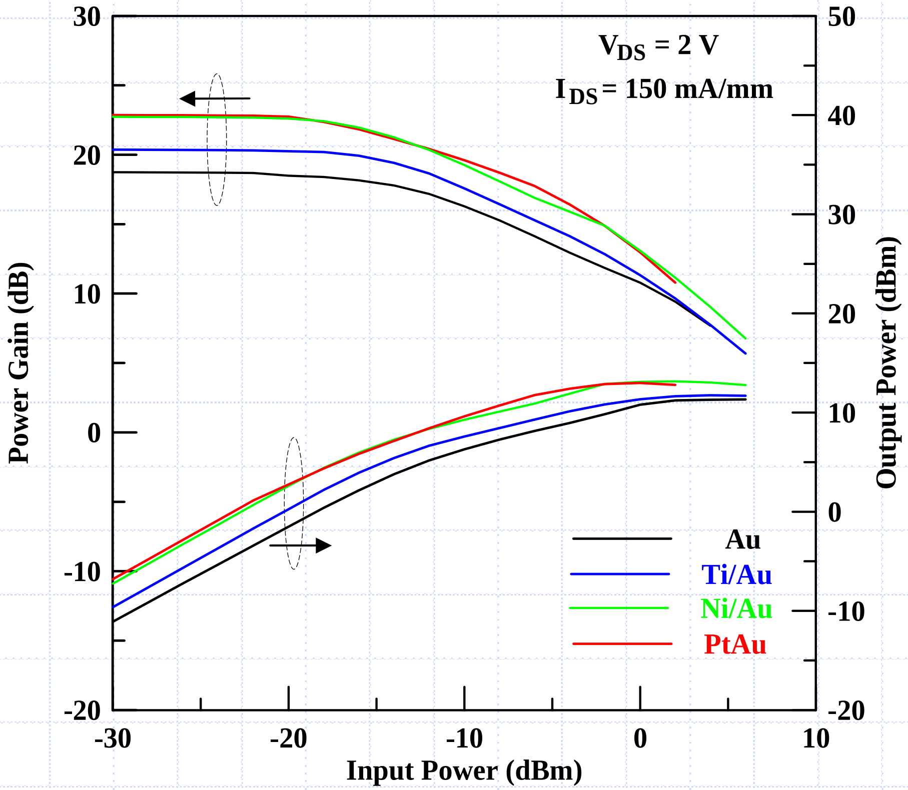

- Due to the largest production of I_{DSS} and BV_{GD}
  - Ni/Au, Pt/Au gates : improved power characteristics

Gate-Alloys-Related Kink Effects

Noise characteristics:

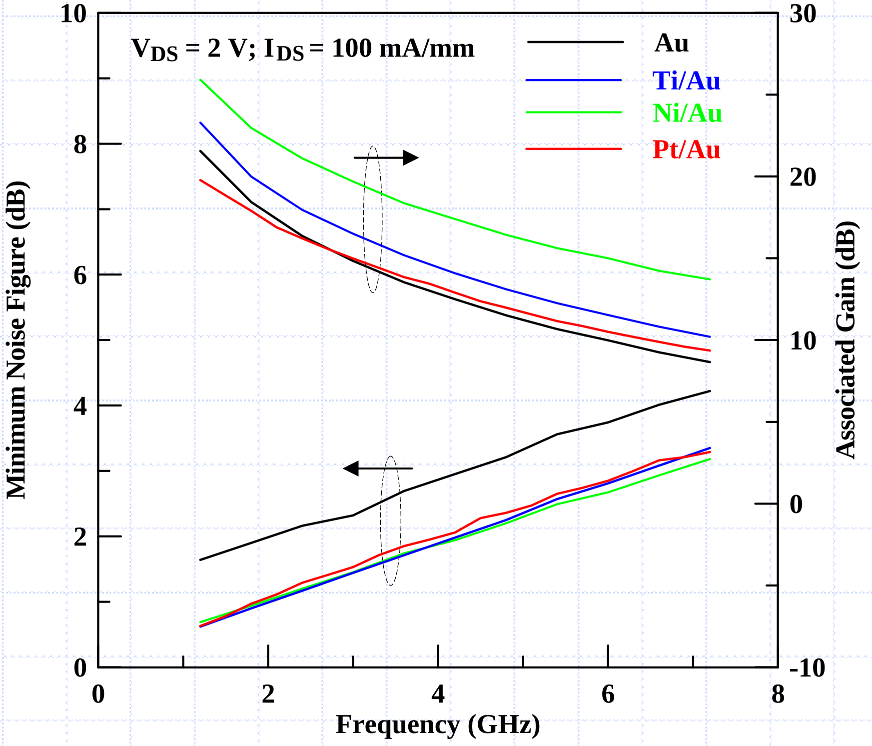

- Due to improved kink effect and output conductance

- Ti/Au, Ni/Au, Pt/Au demonstrate better noise characteristics than Au.

Gate-Alloys-Related Kink Effects

- **Characteristics comparisons by depositing various gate alloys :**

Gate Alloys	Au	Ti/Au	Ni/Au	Pt/Au
f_t (GHz)	17.2	23.8	23.8	20.2
f_{max} (GHz)	29.1	44.9	45.3	53.7
G_s (dB)	18.7	20.3	22.7	22.8
P_{out} (dBm)	11.26	11.74	13.14	12.97
NF_{min} (dB)	2.16	1.17	1.2	1.29
G_a (dB)	16.36	17.96	21.1	16.21

III. Conclusions

- $In_{0.425}Al_{0.575}As/In_{0.65}Ga_{0.35}As$ PC-MHEMT:
  - Better microwave characteristics
    - suitable for high-speed application
  - Noise characteristics
    - suitable for low-noise application
  - Thermal stability
    - suitable high-temperature application

- $In_{0.425}Al_{0.575}As/In_xGa_{1-x}As$ SGC-MHEMT:
  - Power characteristics
    - suitable for high-power application
  - Gate voltage swing
    - suitable for high-linearity application

III. Conclusions

- High Schottky barrier height gate alloys provide effective ways of improving the respective device performances, including the noise, voltage and power gains.

- Complete and efficient high-frequency parameters extraction for RF model build-up facilitates the MMIC application based on the specific MHEMT designs.

- Prosperity of academic studies on MHEMT designs for MMIC applications are promisingly expected.

Q & A

~ The End ~

Many thanks !!

For more discussions, Feel free contact our lab.

by

Email: cslee@fcu.edu.tw

Reference Table